1	
2	Dominant Clade-featured SARS-CoV-2 Co-occurring Mutations Reveals Plausible
3	Epistasis: An in silico based Hypothetical Model
4	
5 6 7	A. S. M. Rubayet Ul Alam <sup>1#</sup> , Ovinu Kibria Islam <sup>1#</sup> , Md. Shazid Hasan <sup>1</sup> , Mir Raihanul Islam <sup>2</sup> , Shafi Mahmud <sup>3</sup> , Hassan M. Al□Emran <sup>4</sup> , Iqbal Kabir Jahid <sup>1</sup> , Keith A. Crandall <sup>5</sup> , M. Anwar Hossain <sup>6,7*</sup>
8	
9 10	1 Department of Microbiology, Jashore University of Science and Technology, Jashore-7408, Bangladesh
11	2 BRAC James P Grant School of Public Health, BRAC University, Bangladesh
12	3 Genetic Engineering and Biotechnology, University of Rajshahi, Rajshai-6205, Bangladesh
13 14	4 Department of Biomedical Engineering, Jashore University of Science and Technology, Jashore-7408, Bangladesh
15 16 17	5 Computational Biology Institute and Department of Biostatistics & Bioinformatics, Milken Institute School of Public Health, The George Washington University, Washington, DC, USA
18	6 Jashore University of Science and Technology, Jashore-7408, Bangladesh
19	7 Department of Microbiology, University of Dhaka, Dhaka-1000, Bangladesh
20	
21	*Correspondence
22 23	M. Anwar Hossain, Jashore University of Science and Technology, Jashore-7408, Bangladesh.
24	E-mail: hossaina@du.ac.bd, Contact: +8801715363753
25	
26	
27	# Authors contributed equally

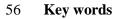
1

28

### 29 ABSTRACT

30 SARS-CoV-2 is evolved into eight fundamental clades where four (G, GH, GR, and GV) are 31 globally prevalent in 2020. How the featured co-occurring mutations of these clades are 32 linked with viral fitness is the main question here and we thus proposed a hypothetical model 33 using *in silico* approach to explain the plausible epistatic effects of those mutations on viral 34 replication and transmission. Molecular docking and dynamics analyses showed the higher 35 infectiousness of a spike mutant through more favorable binding of  $G_{614}$  with the elastase-2. 36 RdRp mutation p.P323L significantly increased genome-wide mutations (p<0.0001) since 37 more flexible RdRp (mutated)-NSP8 interaction may accelerate replication. Superior RNA 38 stability and structural variation at NSP3:C241T might impact protein and/or RNA 39 interactions. Another silent 5'UTR:C241T mutation might affect translational efficiency and 40 viral packaging. These four G-clade-featured co-occurring mutations might increase viral 41 replication. Sentinel GH-clade ORF3a:p.Q57H constricted ion-channel through inter-42 transmembrane-domain interaction of cysteine(C81)-histidine(H57) and GR-clade 43 N:p.RG203-204KR would stabilize RNA interaction by a more flexible and hypo-44 phosphorylated SR-rich region. GV-clade viruses seemingly gained the evolutionary 45 advantage of the confounding factors; nevertheless, N:p.A220V might modulate RNA 46 binding with no phenotypic effect. Our hypothetical model needs further retrospective and 47 prospective studies to understand detailed molecular events featuring the fitness of SARS-48 CoV-2.

- 49
- 50
- 51
- 52
- 53
- 54
- 55



SARS-CoV-2, COVID-19, Infection Paradox, Fitness, Virulence, Clades, Co-occurring
 mutations

59

### 60 **1. Introduction**

61 Severe acute respiratory syndrome coronavirus 2 (SARS-CoV-2), the etiological agent of 62 COVID-19 pandemic, has gained some extraordinary attributes that make it extremely 63 infectious: High replication rate, large burst size, high stability in the environment, strong 64 binding efficiency of spike glycoprotein (S) receptor-binding domain (RBD) with human 65 angiotensin-converting enzyme 2 (ACE2) receptor, and additional furin cleavage site in S protein<sup>1-3</sup>. In addition to those, it has proofreading capability ensuring relatively high-fidelity 66 replication<sup>4</sup>. The virus contains four major structural proteins: spike glycoprotein (S), 67 68 envelope (E), membrane (M), and nucleocapsid (N) protein along with 16 nonstructural 69 proteins (NSP1 to NSP16) and seven accessory proteins (ORF3a, ORF6, ORF7a, ORF7b, ORF8a, ORF8b, and ORF10)<sup>5,6</sup>. Mutational spectra within the SARS-CoV-2 genome<sup>7,8</sup>, spike 70 protein<sup>9</sup>, RdRp<sup>10</sup>, ORF3a<sup>11</sup>, and N protein<sup>12</sup> were reported. 71

72 SARS-CoV-2 was classified into eight major clades, such as G, GH, GR, GV, S, V, L, 73 and O by global initiative on sharing all influenza data (GISAID) consortium (https://www.gisaid.org/) based on the dominant core mutations in genomes where four 74 clades (G, GH, GR, and GV) are globally and geographically prevalent in 2020<sup>13</sup>. Yin <sup>14</sup> 75 76 reported that the 5 UTR mutation 241C > T is co-occurring with three other mutations, 77 3037C > T (NSP3: C318T), 14408C > T (RdRp: p.P323L), and 23403A > G (S: p.D614G). 78 GISAID referred to these co-occurring mutations containing viruses as clade G (named after the spike D614G mutation) or PANGO (<u>https://cov-lineages.org/</u>) lineage B.1<sup>15,16</sup>. The GR 79 80 clade or lineage B.1.1.\* is classified with additional trinucleotide mutations at 28881-28883 81 (GGG>AAC); creating two consecutive amino acid changes, R203K and G204R, in N 82 protein. Another derivative of G clade is GH or lineage B.1.\*, characterized by an additional ORF3a:p.Q57H mutation. The variant GV or lineage B.1.177 featured an A222V mutation in 83 the S protein along with other mutations of the clade G<sup>13,16</sup>. Also, N: A220V, ORF10: V30L 84 85 and three other synonymous mutations T445C, C6286T, and C26801G are observed for this clade<sup>17</sup>. 86

87 The most frequently observed mutation is D614G of the S protein<sup>18</sup>, which has direct roles 88 in receptor binding, and immunogenicity, thus viral immune-escape, transmission, and 89 replication fitness<sup>19,20</sup>. Mutations in proteins other than spike could also affect viral 90 pathogenicity and transmissibility, but the role of those dominant clade-featured mutations 91 has remained largely underestimated. Although the possible role of ORF3a:p.Q57H in 92 replication cycle<sup>21</sup> has recently been investigated, the molecular perspective was not fully 93 explained there. The effect of 5'UTR: C241T, Leader: T445C, NSP3: C318T, RdRp:p.P323L, 94 N:p.RG203-203KR, and N:p.A220V is still being overlooked.

95 Different mutation(s) of SARS-CoV-2 may work independently or through epistatic interactions<sup>22,23</sup>; however, it is difficult to determine exactly how these co-occurring 96 mutations, if not all, might have gained their selective evolutionary fitness<sup>22,24,25</sup>. Hence, 97 many hypothetical questions remain: What are the impacts of these mutations on protein 98 99 structures, and what can be their functional roles? How might these mutated proteins interact 100 together? Is there any possible role of the co-occurring 'silent' mutation? Could these 101 mutations have any plausible impact on viral fitness and virulence? We attempt here to 102 answer these questions by in silico molecular insights of SARS-CoV-2 mutants and possible 103 interactions of proteins containing co-occurring mutations. Overall, this study aims to 104 determine plausible individual and/or epistatic impacts of those mutants during replication in 105 terms of viral entry and fusion, evasion of host cell lysis, replication rate, ribonucleoprotein 106 stability, protein-protein interactions, translational capacity, and ultimately the probable 107 combined effect on viral transmission and fitness.

108 **2. Materials and Methods** 

### 109 **2.1 Retrieval of Sequences and Mutation Analyses**

This study analyzed 225,526 high-coverage (<1% Ns and <0.05% unique amino acid mutations) and complete (>29,000 nucleotides) genome sequences from a total of 3,16,166 sequences submitted to GISAID from January 01, 2020, to January 03, 2021. We removed the non-human host-generated sequences during dataset preparation. The Wuhan-Hu-1 (Accession ID- NC\_045512.2) isolate was used as the reference genome.

A python script (<u>https://github.com/hridoy04/counting-mutations</u>) was used to partition a significant part of the dataset into two subsets based on the RdRp: C14408T mutation and estimated the genome-wide variations (single nucleotide changes) for each strain. For the genome-wide mutation analysis, a total of 37,179 sequences (RdRp wild type or 'C' variant: 9,815; and mutant or 'T' variant: 27,364) were analyzed from our dataset. The frequency of mutations was tested for significance with the Wilcoxon signed-rank test between RdRp 'C'
variant and 'T' variant using IBM SPSS statistics 25.

# 122 2.2 Stability, Secondary and Three-Dimensional Structure Prediction Analyses 123 of S, RdRp, ORF3a, and N Proteins

DynaMut<sup>26</sup> and FoldX 5.0<sup>27,28</sup> were used to determine the stability of both wild and 124 mutant variants of N, RdRp, S, and ORF3a proteins. PredictProtein<sup>29</sup> was utilized for 125 126 analyzing and predicting the possible secondary structure and solvent accessibility of both 127 wild and mutant variants of those proteins. The SWISS-MODEL homology modeling 128 webtool<sup>30</sup> was utilized for generating the three-dimensional (3D) structures of the RdRp, S, 129 and ORF3a protein using 7c2k.1.A, 6xr8.1.A, and 6xdc.1.A PDB structure as the template, respectively. Modeller v9.25<sup>31</sup> was also used to generate the structures against the same 130 templates. I-TASSER<sup>32</sup> with default protein modeling mode was employed to construct the N 131 132 protein 3D structure of wild and mutant type since there was no template structure available 133 for the protein. The built-in structural assessment tools (Ramachandran plot, MolProbity, and Quality estimate) of SWISS-MODEL were used to check the quality of generated structures. 134

# 135 2.3 Molecular Docking and Dynamics of RdRp-NSP8 and Spike-Elastase2 136 Complexes

137 Determination of the active sites affected by binding is a prerequisite for docking 138 analysis. We chose 323 along with the surrounding residues (315-324) of RdRp and the 139 residues 110 to 122 of NSP8 monomer as the active sites based on the previously reported structure<sup>33</sup>. The passive residues were defined automatically where all surface residues were 140 141 selected within the 6.5°A radius around the active residues. The molecular docking of the 142 wild and predicted mutated RdRp with the NSP8 monomer from the PDB structure 7C2K was performed using the HADDOCKv2.4 to evaluate the interaction<sup>34</sup>. The binding affinity 143 of the docked RdRp-NSP8 complex was predicted using the PRODIGY<sup>35</sup>. The number and 144 145 specific interfacial contacts (IC) for each of the complexes were identified.

The human neutrophil elastase (hNE) or elastase-2 (PDB id: 5A0C) was chosen for docking of the S protein, based on earlier reports<sup>36</sup>. Here we employed CPORT<sup>37</sup> to find out the active and passive protein-protein interface residues of hNE. The S protein active sites were chosen based on the target region (594-638) interacting with the elastase-2. The passive residues of S protein were defined automatically as mentioned for RdRp-NSP8 docking analysis. Afterward, we individually docked wild (614D) and mutated (614G) S protein with the hNE using HADDOCK 2.4. The binding affinity of the docked complexes, as well as the number and specific interfacial contacts (IC), were predicted as performed after RdRP-NSP8 docking. We employed HDOCK server<sup>38</sup> with specifying the active binding sites residues for predicting the molecular docking energy.

156 The structural stability of the above-mentioned protein complexes (RdRP-NSP8 and 157 Spike-Elastase2) and their variations were assessed through YASARA Dynamics software 158 package (Land & Humble, 2018). We used AMBER14 force field (Dickson et al., 2014) for 159 these four systems, and the cubic simulation cell was created with the TIP3P (at 0.997 g/L-1, 160 25C, and 1 atm) water solvation model. The PME or particle mesh Ewald methods were applied to calculate the long-range electrostatic interaction by a cut-off radius of 8Å<sup>39</sup>. We 161 applied the Berendsen thermostat to maintain the temperature of the simulation cell. The time 162 step of the simulation was set as 1.25fs<sup>40</sup> and the simulation trajectories were saved after 163 every 100ps. Finally, we conducted the molecular dynamics simulation for 100ns<sup>41-44</sup>. 164

# 165 2.4 Mutational Analysis of Transmembrane Domain 1 of ORF3a and serine-rich 166 (SR) domain of N protein

167 The complete genome of 12 pangolin-derived coronavirus strains, as well as 38 bats, 168 civet, and human SARS-CoVs, were downloaded from GISAID and NCBI, respectively for 169 the mutational comparison between the SARS-CoV and SARS-CoV-2. We mainly targeted 170 transmembrane domain 1 (TM1), which covers 41 to 63 residues, of ORF3a to find the 171 identical mutation and scan overall variation in TM1. A generalized comparison between 172 SARS-CoV and SARS-CoV-2 reference sequences was performed to identify the mutations 173 in the SR-rich region that will help to postulate on N protein functions of novel coronavirus 174 based on previous related research on SARS-CoV.

### 175

### 2.5 Analyzing RNA Folding prediction of 5 UTR, Leader protein, and NSP3

The Mfold web server<sup>45</sup> was used with default parameters to check the folding pattern of 176 177 RNA secondary structure in the mutated 5 UTR, synonymous leader (T445C), and NSP3 178 region (C3037T). The change C6286T is in between the nucleic acid-binding (NAB) domain 179 and betacoronavirus specific marker (\betaSM) domain of the NSP3 region. The change 180 C26801G is at the transmembrane region 3 (TM3) of the virion membrane. Thus, changing in 181 C6286T and C26801G will not affect the function significantly and was not predicted here. The structure of complete mutant 5'UTR (variant 'T') was compared with the wild type 182 (variant 'C') secondary pattern as mentioned in the Huston et al. (2021) <sup>46</sup>. From the Mfold 183

184 web server, we also estimated free energy change ( $\Delta G$ ) for wild and mutant leader and NSP3

- 185 RNA fold to find any variation in stability.
- 186

### 3. RESULTS AND DISCUSSION

187 . The possible individual effects of a total nine mutations in S, RdRp, ORF3a, N, 5'UTR, 188 leader protein (NSP1), and NSP3 in viral replication cycle and transmission were discussed 189 with associated results. Zeng et al. (2020) showed the links of these mutations towards 190 possible epistatic effects on fitness using statistical analysis that duly suits our purpose of presenting how the mutations might play the combined roles<sup>23</sup>. Whereas researches on 191 molecular docking of the spike protein<sup>47,48</sup> and RdRp<sup>49,50</sup> in search of potential drug targets is 192 193 a continuous process, our study approached in a unique way to dock spike with elastase-2 and 194 RdRp with NSP8 to satisfy our purposes. The overall epistatic interactions of the mutant 195 proteins and/or RNA was then depicted (Figure 1) as a hypothetical model and discussed.

### 196 3.1 Spike Protein D614G Mutation Favors Elastase-2 Binding

197 This study found interesting structural features of the S protein while comparing and 198 superimposing the wild protein (D<sub>614</sub>) over mutated protein (G<sub>614</sub>). The secondary structure 199 prediction and surface accessibility analyses showed that there was a slight mismatch at the S1-S2 junction ( $^{681}$ <u>PRRA</u>R $\downarrow$ S $^{686}$ ) where serine at 686 (S $^{686}$ ) was found covered in G<sub>614</sub> and 200 exposed to the surface in  $D_{614}$ . However, S<sup>686</sup> in both  $G_{614}$  and  $D_{614}$  were exposed to an open-201 202 loop region to have possible contact with the proteases (supplementary Figure S1). Further 203 investigation on the aligned 3D structures however showed no conformational change at the 204 S1-S2 cleavage site (Figure 2c). We also observed no structural variation in the surrounding 205 residues of the protease-targeting S1-S2 site (Figure 2c), which eliminated the assumption of Phan<sup>51</sup>. The predictive 3D models and structural assessment of  $D_{614}$  and  $G_{614}$  variants 206 confirmed that the cleavage site at 815-16 of S2 subunit ( $^{812}$ PSKR $\downarrow$ S $^{816}$ ) or S2 $^{1,52}$  had no 207 208 structural and surface topological variation (Figure 2d-e). Rather, the superimposed 3D 209 structures suggested a conformational change in the immediate downstream region  $(^{618}$ TEVPVAIHADQLTPT<sup>632</sup>) of the 614<sup>th</sup> position of mutated protein (G<sub>614</sub>) that was not 210 observed in D<sub>614</sub> variants (Figure 2a-b). 211

Several experiments suggested that mutated ( $G_{614}$ ) protein contains a novel serine protease cleavage site at 615-616 that is cleaved by host elastase-2, a potent neutrophil elastase, level of which at the site of infection during inflammation will facilitate the host cell entry for  $G_{614}^{18,36,53,54}$ . The elastase-2 restrictedly cut valine at 615, due to its valine-

dependent constriction of catalytic groove<sup>55</sup>. The present sequence setting surrounding  $G_{614}$ 216 (P6-<sup>610</sup>VLYQGV1NCTEV<sup>620</sup>-P'5) showed a higher enzymatic activity on the spike<sup>36</sup>, which 217 218 cannot be completely aligned with the previous works on the sequence-based substrate 219 specificity of elastase- $2^{56}$ . However, the first non-aligned residue of the superimposed G<sub>614</sub>, located at the P'4 position ( $T^{618}$ ), may also be important for binding with the elastase-2, and 220 221 further down the threonine (T) at 618, the residues may affect the bonding with the respective 222 amino acids of elastase-2 (Figure 2a-b). This changed conformation at the downstream binding site of  $G_{614}$  may help overcome unfavorable adjacent sequence motifs around  $G^{614}$ 223 residue. Therefore, the simultaneous or sequential processing of the mutated S protein by 224 225 TMPRSS2/Furin/Cathepsin and/or elastase-2 facilitates a more efficient SARS-CoV-2 entry into the host cells and cell-cell fusion<sup>36,53,54</sup>. 226

227 This study further observed the possible association of the S protein with elastase-2 228 and found an increased binding affinity in case of  $G_{614}$  (Table 1). Hence, the active sites of 229 the mutated protein interacted efficiently with more amino acids of elastase-2 (Table 2), 230 possibly providing a better catalytic activity as shown by Hu et al. (2020)<sup>36</sup>. The mutation 231 may have changed the structural configuration of the elastase-2 cleavage site in a way that the 232 enzyme is facing less challenge to get near to the cutting site of the altered protein (Figure 2a-233 b and 3). The efficient cleaving of this enzyme, although located in an upstream position of 234 the S1-S2 junction, may assist in releasing S1 from S2 and change the conformation in a way 235 that later help in cleaving at the S2' site by other protease(s) before fusion 57,58. Mutated spike 236 protein and elastase-2 complex was more flexible than the wild spike-elastase complex, and 237 the interactions with enzyme was also different as shown in RMSD deviation between the 238 complexes (Figure 4).

This G<sup>614</sup> amino acid replacement may have a destabilization effect on the overall 239 protein structure (Table 2 and Figure 2a-b). The deformed flexible region at or near G<sup>614</sup> is 240 the proof of that destabilizing change (Figure 2f and supplementary figure S3). Zhang et al.<sup>59</sup> 241 explained less S1 shedding through more stable hydrogen bonding between  $Q^{613}$  (glutamine) 242 and  $T^{859}$  (threenine) of protomer due to greater backbone flexibility provided by  $G^{614}$ . 243 244 Moreover, G614 mutation may increase S protein stability and participate in N-linked glycosylation at N616<sup>36</sup>. On the other hand, increasing the number of RBD up conformation 245 246 or increasing the chance of 1-RBD-up conformation due to breakage of both intra-and inter-247 protomer interactions of the spike trimer and symmetric conformation will give a better 248 chance to bind with ACE2 receptor and can also increase antibody-mediated neutralization<sup>60</sup>.

249 The S1 will release from S2 more effectively in  $G_{614}$  protein by introducing glycine that will break hydrogen bond present in between the D<sup>614</sup> (wild) and T<sup>859</sup> (threonine) of the 250 neighboring protomer<sup>60,61</sup>. Our analyses have provided the *in silico* proof of this later fact by 251 252 showing that the mutated protein was more flexible than the wild type protein by missing a hydrophobic interaction between  $G^{614}$  and  $Phe^{592}$  (Figure 2g-h). This new adjunct result 253 accorded well with Weismann et al. (2020) that  $G^{614}$  will increase overall flexibility of the 254 255 mutated protein. The overall structural change may assist the mutated S protein by providing 256 elastase-2 a better binding space and attachment opportunity onto the cleavage site (Figure 257 3a-b), thus providing a more stable interaction that increases the credibility of an efficient 258 infection (Figure 1).

# 3.2 Increased Flexibility of RdRp-NSP8 Complex: Compromise Proof-Reading Efficiency with Replication Speed

261 The binding free energy ( $\Delta G$ ) of the RdRp-NSP8 complexes have been predicted to 262 be -10.6 and -10.5 Kcalmol<sup>-1</sup>, respectively, in wild ( $P_{323}$ ) and mutated ( $L_{323}$ ) type that 263 suggests a more flexible interaction for the mutated protein (Table 2). The increased number 264 of contacts found in the  $L_{323}$ -NSP8 complex (Table 1) were possibly due to slightly more 265 hydrogen bonds, which had no considerable impact on protein flexibility (Figure 4d). Our analyses identified that proline  $(P^{323})$  or leucine  $(L^{323})$  of RdRp can interact with the aspartic 266 acid (D<sup>112</sup>), cysteine (C<sup>114</sup>), valine (V<sup>115</sup>), and proline (P<sup>116</sup>) of NSP8 (Table 1 and Figure 5). 267 RdRp binds with NSP8 in its interface domain (from residues alanine: $A^{250}$  to arginine: $R^{365}$ ), 268 forming positively charged or comparatively neutral 'sliding poles' for RNA exit, and 269 enhance the replication speed probably by extending the RNA-binding surface in that domain 270 area<sup>62,63</sup>. Molecular dynamics of the mutated RdRp-NSP8 complex supported this by showing 271 272 a more expanded surface area in the interacting site (Figure 4b) and maintained integrity 273 throughout the simulation (Figure 4c). Besides, we did not find any interaction of NSP8 with the zinc-binding residues  $(H^{295}, C^{301}, C^{306} \text{ and } C^{310})$  of the RdRp protein (Table 3 and Figure 274 5)<sup>64,65</sup>. Therefore, the P323L mutation within this conserved site of the RdRp interface 275 276 domain may only affect the RdRp-NSP8 interaction without changing metal binding affinity.

277 The results from six state-of-the-art tools of protein stability suggested that mutated 278 (L<sub>323</sub>) protein cannot be concluded as 'stable', only because of ambiguous  $\Delta\Delta G$  estimates 279 (Table 2), rather the interaction with the adjacent amino acid mainly defined the stability<sup>66</sup>. 280 The superimposed 3D structures and secondary structure analyses showed that there was no

deviation in loop/turn structure of mutated protein, even though hydrophobic leucine ( $L^{323}$ ) 281 282 was embedded (supplementary Figure S1 and S4). To some extent, the mutation stabilized 283 the  $L_{323}$  structure making the protein more rigid and binds less strongly with the NSP8 by 284 expanding the interacting region. These variations may together increase the replication speed 285 by helping exit the processed RNA genome from the RdRp groove structure more swiftly 286 (Figure 1). The increasing replication speed might be due to the perturbation of interaction between RdRp and NSP8<sup>62,66</sup>, or less possibly, the complex tripartite interactions (RdRp, 287 NSP8, and NSP14) responsible for the speculated decrease of proof-reading efficiency<sup>4</sup>. 288 289 Thus, RdRp mutants might increase the mutation rate by a trade-off between high replication speed and low fidelity of the mutated polymerase<sup>67</sup>. Another possibility could be the lower 290 proof-reading efficiency of NSP14 that was however not linked to the replication speed<sup>4</sup>. 291 292 Analysis of our study sequences revealed that the frequency of mutation (median=8) in  $L_{323}$ 293 mutants (n=27,364) is significantly higher (p<0.0001) than the frequency (median=6) of 294 wild-type  $(P_{323})$  strains (n=9,815). This increased mutation rate may play a vital role in 295 genetic drifts and provide next generations a better adaptation to adverse environments.

#### 296

### 3.3 Q57H Substitution in ORF3a Viroporin: The Roles of Decreased Ion Permeability

This study has found that the replacement of glutamine  $(Q^{57})$  with positively charged 297 histidine (H<sup>57</sup>) at 57 position of ORF3a transmembrane region 1 (TM1) does not change 298 299 secondary transmembrane helical configuration (supplementary Figure S1), and aligned 3D 300 structures have also shown no variation of TM1 in the monomeric state (Figure 6a). The 301 mutant (H<sub>57</sub>) protein has a non-significant increase in structural stabilization and a minimal 302 decrease in molecular flexibility (Table 2 and supplementary Figure S5). This is because of the weak ionic interaction of  $H^{57}$ - $C_{\alpha}$  with the sulfur atom of cysteine ( $C^{81}$ ) that is present in 303 TM2 and the hydrogen bond of terminal  $N_{\zeta}$  of lysine (K<sup>61</sup>) with one of the endocyclic 304 nitrogens of H<sup>57</sup> (Figure 6b). The Q<sup>57</sup> in wild-type protein forms the major hydrophilic 305 constriction within the ORF3a channel pore<sup>68</sup>. Thus, further favorable increasing 306 constrictions within the  $H_{57}$  protein channel pore due to diagonal  $H^{57}$  (TM1)- $C^{81}$  (TM2) ionic 307 308 interaction (Figure 6b) and the replacement of charge-neutral glutamine with a positively 309 charged histidine in the selectivity filter may reduce the passing of positive ions, such as  $Ca^{2+}$ ,  $Na^{+}$ , and  $K^{+}$ , by either electrostatic repulsion or blocking<sup>69-72</sup>. This speculation for 310 ORF3a mutated protein was supported by another study showing the reduction of ion 311 permeability of Na<sup>2+</sup> and Ca<sup>2+</sup> through the H<sub>57</sub>, however, that decrease was not found 312 313 statistically significant  $(p>0.05)^{68}$ .

The decrease intracellular concentration of cytoplasmic  $Ca^{2+}$  ions potentially reduces 314 caspase-dependent apoptosis of the host cell<sup>73</sup>, mainly supporting viral spread without 315 affecting replication<sup>21</sup> as shown in Figure 1. Moreover, the ORF3a can drive necrotic cell 316 death<sup>74</sup> wherein the permeated ions into cytoplasm<sup>75</sup> and the insertion of ORF3a as viroporin 317 into lysosome<sup>76</sup> play vital roles. The  $H_{57}$  mutant may thus decrease pathogenicity and 318 319 symptoms during the early stages of the infection, i.e., reducing 'cytokine storm' in the host<sup>77</sup>. Besides, ORF3a was proved to affect inflammasome activation, virus release, and cell 320 death, as shown by Castaño-Rodriguez et al. (2018)<sup>78</sup> that the deletion of ORF3a reduced 321 viral load and morbidity in animal models. 322

323 Even though similar proteins of ORF3a have been identified in the sarbecovirus lineage infecting bats, pangolins, and humans<sup>79</sup>, only one pangolin derived strain from 2017 324 in Guangxi, China contains  $H^{57}$  residue as shown by mutation analyses (supplementary 325 Figure S5), and also reported by Kern et al. (2020)<sup>68</sup>. The presence of this mutation in 326 327 pangolin could be an accidental case or might explain its impact on modulating host-specific 328 immune response, which needs functional experimental verification. A possible explanation 329 behind that presence could be the more adaptive nature of the virus towards reverse 330 transmission by being less virulent, i.e., from human to other animals, as observed in recent reports<sup>80,81</sup>. 331

# 332 3.4 N Protein Mutation: Augmenting Nucleocapsid Stability and Exerting 333 Miscellaneous Effects

Our study has observed that the combined mutation (N: p.RG203-204KR) causes no conformational change in secondary and 3D structures (Figure S1 and Figure 7, respectively) of the conserved SR-rich site (184  $\rightarrow$  204) in the linker region (LKR: 183  $\rightarrow$  254) of the N protein (supplementary Figure S7), but there is a minor alteration among buried or exposed residues (supplementary Figure S1c and Figure 8b). The superimposed 3D structures showed structural deviation, rather at <sup>231</sup>ESKMSGKGQQQQGQTVT<sup>247</sup> of the LKR (Figure 7), corresponding to the high destabilization of the mutated (KR<sub>203-204</sub>) protein (Table 2).

Impedance to form particular SR-motif due to  $RG \rightarrow KR$  mutation might disrupt the phosphorylation catalyzed by host glycogen synthase kinase-3<sup>82</sup>. After virus enters into the cell, this synchronized hypo-phosphorylation of  $KR_{203-204}$  protein should make the viral ribonucleoprotein (RNP) unwind in a slower but more organized fashion that might have an impact upon translation and immune-modulation<sup>83-85</sup>. In  $KR_{203-204}$ , replacement of glycine 346 with arginine may increase the nucleocapsid (N protein-RNA complex) stability by forming stronger electrostatic and ionic interactions due to increased positive charge<sup>86,87</sup>. Besides, the 347 more disordered orientation of the downstream LKR site<sup>83</sup> and highly destabilizing property 348 of KR<sub>203-204</sub> may assist in the packaging of a stable RNP<sup>88,89</sup>. N protein also utilizes the 349 350 dynamic nature of the intrinsically disordered linker region (LKR) that controls its affinity towards M protein, self-monomer, 5'UTR, and cellular proteins<sup>90-92</sup>. The phosphorylation at 351 the LKR site may play an essential role to regulate these interactions<sup>86</sup>. These plausible 352 353 interactions and impact upon mutations are depicted in Figure 1.

354 **3.5** 

### 3.5 Silent Mutations may not be Silent

The C241T of 5'UTR (untranslated region), a single nucleotide 'silent' mutation, is located at the UUCGU pentaloop part of the stem-loop region (SLR5B). This pentaloop of 5'UTR remains unchanged and maintains a particular structure with a potential role in viral packaging<sup>91,93</sup>. The RNA secondary structural analysis in our study predicted that there is no change in the 241T structure (supplementary Figure S8a). However, C241T is present just upstream to the ORF1a start codon (266-268 position) and may be involved in differential RNA binding affinity to the ribosome and translational factors<sup>94</sup>.

362 In the case of multi-domain NSP3 (papain-like protease), we have observed superior 363 stability of the RNA after gaining the synonymous mutation 3037C<T (C318T) where wild 364 and mutant RNA structure has -151.63 and -153.03 Kcal/mol, respectively (Supplementary 365 Figure S7b-c). A more stable secondary structure of (+)-ssRNA as observed in the mutated 366 NSP3 protein coding sequence corresponds to the slower translational elongation that generally contributes to a range of abnormalities resulting in low translation efficiency 367 affecting posttranslational modifications as a part of protein regulation<sup>95</sup>. This silent mutation 368 369 is located within the flexible loop of the NSP3 ubiquitin-like domain 1 (Ubl1). In SARS-370 CoV, Ubl1 was reported to bind with single-stranded RNA containing AUA patterns and interact with the nucleocapsid (N) protein<sup>96,97</sup>. Besides, Ubl1 was likely to bind with several 371 signature repeats in 5'-UTR in SARS-CoV-2 genome<sup>98</sup>. Finally, change in T445C in leader 372 373 protein may not cause any change in expression or others since the structure (data not shown) 374 and energy are same -172.34 kcal/mol. Figure 1 represents the overall possible scenario due 375 to these silent mutations.

## 376 3.6 Epistatic Effects of the Co-occurring Mutations on Viral Replication and 377 Transmission: A Plausible Hypothesis

378 The co-occurring mutations, as defined by the presence of simultaneous multi-site 379 variations in the same or different proteins or in the genome, have provided new insights into 380 the dynamic epistatic network by employing differential molecular interactions. The epistatic 381 effects of the mutations were reported to control viral fitness and virulence through 382 modulating replication cycle and virus-host interactions, as observed before for Influenza and Ebola virus<sup>99-104</sup>. For instance, the detrimental effect of R384G on influenza A fitness was 383 overcome by the co-occurring mutation E375G<sup>100,103</sup>, and co-occurring mutations at the 384 antigenic sites of influenza hemagglutinin can also drive viral evolution<sup>102,104</sup>. The correlation 385 of the co-occurring GP-L mutations affect Ebola virus virulence and thus case fatality rate<sup>101</sup>. 386 387 The co-occurring mutations of the major SARS-CoV-2 clades discussed in this work showed epistatic link<sup>22,23</sup>, and positive selection pressure except for the synonymous mutations<sup>22,24,25</sup> 388 that were also shown in Observable site (https://observablehq.com/). We propose here a 389 390 hypothesis (model) on how the co-occurring mutations of SARS-CoV-2 might influence 391 replication and transmission fitness of the major clade strains.

392 Between two important G clade-featured co-occurring mutations, the p:D614G of the 393 S protein and p:P323L of RdRp, we speculated no interlinked functional relationship (Figure 394 1) and the sequence based prediction showed no potentially significant epistatic link as well<sup>23</sup>. These seemingly unrelated mutations can cumulatively escalate the infectiousness of 395 396 the virus as a result of higher viral load and shorter burst time. The S:p.D614G might assist in 397 rapid entry into the host cells with an efficient elastase-2 activity and higher transmissibility and/or aggressiveness of  $G_{614}$  mutant<sup>19,20</sup> and could be related to elastase-2 or human 398 neutrophil elastase (hNE) concentration during inflammation<sup>105</sup>. Besides, higher levels of 399 400 functional S protein observed in G614 strains can increase the chance of host-to-host transmission<sup>59</sup>. The RdRp:p:P323L may rather boost up the replication by a faster RNA 401 402 processing (exiting) that can open up the avenue to generate strains with significantly (p<0.0001) higher number of mutations. This increased mutation rate in L<sub>323</sub> mutants can 403 surpass the constant proof-reading fidelity<sup>106</sup> and evolve into a greater number of variants 404 405 within a population (Figure 1), that might help adapt more quickly in adverse climatic condition, evade the immune response, and survive within different selective pressure<sup>107,108</sup>. 406

NSP3 is a scaffolding protein for the replication-transcription complex, and the
possible change in its structure may affect the overall dynamics of viral replication<sup>96,97</sup>.
P323L mutation of RdRp may change binding affinity to the Ubl1 region of NSP3<sup>109</sup> (Figure
Significant epistatic links of NSP3:C3037T with spike and RdRp mutations was also

411 reported by Zeng et al.  $(2020)^{23}$ . In contrast, we could not predict any possible association of 412 the 5 UTR:C241T mutation with the S, RdRp, and NSP3 mutated proteins as also shown by 413 sequence analysis in Zeng et al.  $(2020)^{23}$ . The rapid within-host replication and modified 414 replication dynamics might be correlated with the fitness of G clade strains<sup>110</sup>.

415 The mutant N protein may have an impact on viral replication and transcription, like other coronaviruses<sup>92</sup>, through the binding with NSP3 protein that is linked to RdRp centered 416 417 replication complex. The N protein can also affect the membrane stability by yet 418 uncharacterized interaction with the M protein, which could ultimately produce more stable virion particles<sup>111-113</sup>. A stronger N protein-RNA complex provokes slower intracellular 419 immune response<sup>84</sup>, and at the same time, can still remain highly contagious and aggressive 420 421 because of the concurrent presence of G clade-featured S protein and RdRp mutations (Figure 422 1). The GR strains could hence attain a plausible advantage over G and GH by a more 423 orchestrated, delicately balanced synergistic effects on replication and transmission fitness. 424 These epistatic effects might have increased the fitness by hiding the virus from cellular 425 immunity of the host and increasing stability in the environment, i.e., more transmissible 426 through air and surface. Conversely, we have not found any literature for even other 427 coronaviruses that correlated the ORF3a: p.Q57H with rest of the co-occurring mutations. 428 The H<sub>57</sub> mutant, possibly linked to the mild or asymptomatic cases, may allow the silent 429 transmission and increase the chance of viral spread by lowering the activation of 430 inflammatory response (Figure 1), such as reduced viral particle release and cytokine storm<sup>21,114,115</sup>. 431

The GV strains featuring an A222V mutation in the S protein along with other 432 433 mutations of the clade G was reported to have probably no effect on the viral transmission, 434 severity, and escaping antibody due to its structural position, rather superspreading founder 435 events after lifting up of travel restriction in Europe and lack of effective containment might be the cause of its spreading within  $Europe^{17,116}$ . There was, however, speculation about the 436 437 effect of this mutation on immunogenicity since computational analysis predicted its location within T-cell target region<sup>117,118</sup>. The A220V mutation in the N protein of the GV clade 438 439 showed a slightly more stable formation of the mutated N protein linker region (Table 2) with no change in the chemical properties, that might affect RNA binding affinity<sup>88</sup>, but how this 440 441 change might give an advantage for the GV strains is a question for further experiments. 442 However, different mutations at positions 220 in N found in other major lineages showed no 443 clear evidence of phenotypic consequence (Hodcroft et al., 2020). There was also no 444 epistatically linked pairing between GV clade co-occurring mutations<sup>22,23</sup>. Altogether, the co 445 occurring mutations of GV strains might not affect transmission fitness.

446 Vaccine inequity, immunocompromised patients, and a tremendous number of hosts 447 are now frequently introducing variants with mutations in the receptor binding domain (RBD) 448 of spike protein, i.e., lineage B.1.1.7, a variant of concern under GR clade, consists of 17 449 mutations (14 nonsynonymous and 3 deletions) in spike, N, ORF1ab, and ORF8 proteins, as well as, 6 silent mutations<sup>119,120</sup>. The newly added mutations in this lineage on top of the 450 451 original GR clade-featured ones in the genome might play most crucial role both in 452 increasing transmission fitness and a slightly reduced neutralization to antibody by showing epistatic effects<sup>121121,122</sup>. Other emerging variants (B.1.617.\*, B.1.351, B.1.258, etc.) with 453 454 additional co-occurring mutations are also the descendants of these major clades. Future 455 studies are necessary to investigate the roles of the 'mutation package' present in each of 456 these variants of concern/interest.

### 457 **4. CONCLUSION**

458 In 2020, the course of COVID-19 pandemic was dominated by the G, GH, GR, and GV 459 clades. The G clade-featured co-occurring mutations might increase the viral load, alter 460 immune responses in host and modulate intra-host virus genome plasticity that arises the 461 speculation of their probable role in frequent transmission. The GR and GH clade mutant 462 with the signature mutation, respectively, in nucleocapsid and ORF3a protein might 463 contribute to immune response of the host and viral transmission. The GV strains however 464 could have spread quickly by superspreading events with no apparent epistatic effect. 465 Therefore, the fitness of SARS-CoV-2 may increase in terms of replication and transmission 466 where viral strains are always giving their spread capacity within a population the top priority 467 by calibrating the infection cycle. However, further in vivo and ex vivo studies and more 468 investigations are required to prove and bolster this hypothesis.

469 Data Availability

All the sequence and structural data were taken from the GISAID (<u>https://www.gisaid.org/</u>) and RCSB PDB (https://www.rcsb.org/) as mentioned in the methodology section. We provide all the necessary information such as accession numbers, date-based data source for helping readers and reviewers to check the authenticity of the work.

#### 475 Acknowledgments

15

We would like to acknowledge the team at GISAID for creating SARS-CoV-2 global database. The funding of the research was provided by Jashore University of Science and Technology. We appreciate to the Microbial Genetics and Bioinformatics Laboratory of University of Dhaka for the support of the high-performance computer access. We thanked M. Shaminur Rahman for their technical assistance in protein structure stability analyses.

481

#### Conflict of Interest Statement

482 We have no conflict of interest.

### 483 **Biographical Note**

A. S. M. Rubayet Ul Alam (ASMRUA) is an assistant professor in the Department of
Microbiology, Jashore University of Science and Technology. His research mainly focuses
on molecular biology, data analysis, and bioinformatics.

487 Ovinu Kibria Islam (OKI) is an assistant professor in the Department of
488 Microbiology, Jashore University of Science and Technology. His research activity is
489 focused on molecular biology and big data analysis.

Md. Shazid Hasan (MSH) is an assistant professor in the Department of
Microbiology, Jashore University of Science and Technology. His research activity is
focused on molecular biology and bioinformatics.

Mir Raihanul Islam (MRI) is the Senior Research Associate of BRAC James P Grant School of Public Health, BRAC University who is expert in statistical analysis and epidemiological study and is currently working on many active researches related to public health.

497 Shafi Mahmud (SM) is working as a Master's thesis student in the department of498 Genetic Engineering and Biotechnology, University of Rajshahi, Rajshai-6205, Bangladesh.

Hassan M. Al Emran (HMA) is the Chairman in the Department of Biomedical
Engineering, Jashore University of Science and Technology, Jashore-7408, Bangladesh. His
research mainly focuses on clinical microbiology and infectious diseases.

502 Dr. Iqbal Kabir Jahid (IKJ) is a Professor and Chairman in the Department of 503 Microbiology, Jashore University of Science and Technology. His research mainly focuses 504 on molecular biology. Keith A. Crandall (KAC) is a Professor in the Department of Biostatistics &
Bioinformatics and the director of Computational Biology Institute, Director of Genomics
Core, Milken Institute School of Public Health, The George Washington University,
Washington, DC, USA.

509 M. Anwar Hossain (MAH) is the director of Genome Center, and Vice Chancellor of 510 Jashore University of Science and Technology. He is an expert in molecular biology, 511 virology and vaccine development.

512

### **Authors' Contribution**

513 IKJ, OKI and ASMRUA hypothesized about the work. ASMRUA performed the 514 sequence analysis part after OKI and MSH compiled the dataset. The Python coding, 515 structural (both RNA and protein), and protein docking were done by ASMRUA. MSH 516 predicted protein structure in I-TASSER and performed stability analysis in DynaMut. SM 517 performed the molecular dynamics study. HMA performed the statistical analysis. HMA then 518 reviewed and organized the manuscript expertly. IKJ, KAC and MAH supervised, suggested 519 and revised the write-up to produce the final draft.

### 520 **REFERENCES**

- Hoffmann M, Kleine-Weber H, Pöhlmann S. A multibasic cleavage site in the spike
   protein of SARS-CoV-2 is essential for infection of human lung cells. *Molecular Cell*.
   2020.
- 524 2. Hoque MN, Chaudhury A, Akanda MAM, Hossain MA, Islam MT. Genomic
  525 diversity and evolution, diagnosis, prevention, and therapeutics of the pandemic
  526 COVID-19 disease. *PeerJ*. 2020;8:e9689.
- 527 3. Petersen E, Koopmans M, Go U, et al. Comparing SARS-CoV-2 with SARS-CoV
  528 and influenza pandemics. *The Lancet infectious diseases*. 2020.
- 4. Romano M, Ruggiero A, Squeglia F, Maga G, Berisio R. A Structural View of SARSCoV-2 RNA Replication Machinery: RNA Synthesis, Proofreading and Final
  Capping. *Cells*. 2020;9(5):1267.
- 532 5. Rahman MS, Hoque MN, Islam MR, et al. Epitope-based chimeric peptide vaccine 533 design against S, M and E proteins of SARS-CoV-2 etiologic agent of global 534 pandemic COVID-19: an in silico approach. *PeerJ*. 2020;8:e9572.
- 5356.Yoshimoto FK. The Proteins of Severe Acute Respiratory Syndrome Coronavirus-2536(SARS CoV-2 or n-COV19), the Cause of COVID-19. The protein journal.5372020;39(3):198-216.
- 5387.CallawayE.The coronavirus is mutating-does it matter?Nature.5392020;585(7824):174-177.
- 540 8. Islam MR, Hoque MN, Rahman MS, et al. Genome-wide analysis of SARS-CoV-2
  541 virus strains circulating worldwide implicates heterogeneity. *Scientific reports*.
  542 2020;10(1):1-9.

543 9. Rahman MS, Islam MR, Hoque MN, et al. Comprehensive annotations of the 544 mutational spectra of SARS CoV 2 spike protein: a fast and accurate pipeline. 545 Transboundary and emerging diseases. 2020. 546 10. Eskier D, Karakülah G, Suner A, Oktay Y. RdRp mutations are associated with 547 SARS-CoV-2 genome evolution. PeerJ. 2020;8(e):9587. 548 11. Hassan SS, Choudhury PP, Basu P, Jana SS. Molecular conservation and Differential 549 mutation on ORF3a gene in Indian SARS-CoV2 genomes. Genomics. 2020. 550 12. Shaminur Rahman M, Rafiul Islam M, Rubayet Ul Alam A, et al. Evolutionary 551 dynamics of SARS  $\Box$  CoV  $\Box$  2 nucleocapsid (N) protein and its consequences. Journal 552 of medical virology. 553 13. Hamed SM, Elkhatib WF, Khairalla AS, Noreddin AM. Global dynamics of SARS-554 CoV-2 clades and their relation to COVID-19 epidemiology. Scientific reports. 555 2021;11(1):1-8. 556 14. Yin C. Genotyping coronavirus SARS-CoV-2: methods and implications. Genomics. 557 2020;112(5):3588-3596. 558 15. Mercatelli D, Giorgi FM. Geographic and genomic distribution of SARS-CoV-2 559 mutations. Frontiers in microbiology. 2020;11:1800. 560 Rambaut A, Holmes EC, O'Toole Á, et al. A dynamic nomenclature proposal for 16. 561 SARS-CoV-2 lineages to assist genomic epidemiology. Nature microbiology. 562 2020;5(11):1403-1407. 563 17. Hodcroft EB, Zuber M, Nadeau S, et al. Emergence and spread of a SARS-CoV-2 564 variant through Europe in the summer of 2020. medRxiv. 2020. 565 18. Grubaugh ND, Hanage WP, Rasmussen AL. Making sense of mutation: what D614G 566 means for the COVID-19 pandemic remains unclear. Cell. 2020. 567 19. Plante JA, Liu Y, Liu J, et al. Spike mutation D614G alters SARS-CoV-2 fitness. 568 *Nature*. 2020:1-9. 569 20. Hou YJ, Chiba S, Halfmann P, et al. SARS-CoV-2 D614G variant exhibits efficient 570 replication ex vivo and transmission in vivo. Science. 2020. 571 21. Issa E, Merhi G, Panossian B, Salloum T, Tokajian S. SARS-CoV-2 and ORF3a: 572 Nonsynonymous Mutations, Functional Domains, and Viral Pathogenesis. Msystems. 573 2020;5(3). 574 22. Rochman ND, Wolf YI, Faure G, Mutz P, Zhang F, Koonin EV. Ongoing global and 575 regional adaptive evolution of sars-cov-2. Proceedings of the National Academy of 576 Sciences. 2021;118(29). 577 23. Zeng H-L, Dichio V, Horta ER, Thorell K, Aurell E. Global analysis of more than 578 50,000 SARS-CoV-2 genomes reveals epistasis between eight viral genes. 579 Proceedings of the National Academy of Sciences. 2020;117(49):31519-31526. 580 24. Presti AL, Rezza G, Stefanelli P. Selective pressure on SARS-CoV-2 protein coding 581 genes and glycosylation site prediction. Helivon. 2020;6(9):e05001. 582 Berrio A, Gartner V, Wray GA. Positive selection within the genomes of SARS-CoV-25. 583 2 and other Coronaviruses independent of impact on protein function. PeerJ. 584 2020;8:e10234. 585 26. Rodrigues CH, Pires DE, Ascher DB. DynaMut: predicting the impact of mutations 586 on protein conformation, flexibility and stability. Nucleic acids research. 587 2018;46(W1):W350-W355. 588 27. Schymkowitz J, Borg J, Stricher F, Nys R, Rousseau F, Serrano L. The FoldX web 589 server: an online force field. *Nucleic acids research*. 2005;33(suppl\_2):W382-W388. 590 28. Delgado J, Radusky LG, Cianferoni D, Serrano L. FoldX 5.0: working with RNA, 591 small molecules and a new graphical interface. Bioinformatics. 2019;35(20):4168-592 4169.

- Solution 593 29. Rost B, Yachdav G, Liu J. The predictprotein server. *Nucleic acids research*.
  2004;32(suppl\_2):W321-W326.
- 59530.Waterhouse A, Bertoni M, Bienert S, et al. SWISS-MODEL: homology modelling of596protein structures and complexes. *Nucleic acids research*. 2018;46(W1):W296-W303.
- 597 31. Webb B, Sali A. Comparative protein structure modeling using MODELLER.
  598 *Current protocols in bioinformatics*. 2016;54(1):5.6. 1-5.6. 37.
- 59932.Roy A, Kucukural A, Zhang Y. I-TASSER: a unified platform for automated protein600structure and function prediction. *Nature protocols*. 2010;5(4):725-738.
- Wang Q, Wu J, Wang H, et al. Structural basis for RNA replication by the SARSCoV-2 polymerase. *Cell*. 2020;182(2):417-428. e413.
- 4. Van Zundert G, Rodrigues J, Trellet M, et al. The HADDOCK2. 2 web server: userfriendly integrative modeling of biomolecular complexes. *Journal of molecular biology*. 2016;428(4):720-725.
- 35. Xue LC, Rodrigues JP, Kastritis PL, Bonvin AM, Vangone A. PRODIGY: a web
  server for predicting the binding affinity of protein-protein complexes. *Bioinformatics*. 2016;32(23):3676-3678.
- 609 36. Hu J, He CL, Gao Q, et al. The D614G mutation of SARS-CoV-2 spike protein
  610 enhances viral infectivity. *bioRxiv*. 2020.
- 611 37. de Vries SJ, Bonvin AM. CPORT: a consensus interface predictor and its
  612 performance in prediction-driven docking with HADDOCK. *PloS one*.
  613 2011;6(3):e17695.
- 614 38. Yan Y, Tao H, He J, Huang S-Y. The HDOCK server for integrated protein–protein
  615 docking. *Nature protocols*. 2020;15(5):1829-1852.
- 616 39. Krieger E, Nielsen JE, Spronk CA, Vriend G. Fast empirical pKa prediction by Ewald
  617 summation. *Journal of molecular graphics and modelling*. 2006;25(4):481-486.
- Krieger E, Vriend G. New ways to boost molecular dynamics simulations. *Journal of computational chemistry*. 2015;36(13):996-1007.
- 620 41. Chowdhury KH, Chowdhury M, Mahmud S, et al. Drug Repurposing Approach
  621 against Novel Coronavirus Disease (COVID-19) through Virtual Screening Targeting
  622 SARS-CoV-2 Main Protease. *Biology*. 2021;10(1):2.
- 42. Pramanik SK, Mahmud S, Paul GK, et al. Fermentation optimization of cellulase
  production from sugarcane bagasse by Bacillus pseudomycoides and molecular
  modeling study of cellulase. *Current Research in Microbial Sciences*. 2021;2:100013.
- 43. Swargiary A, Mahmud S, Saleh MA. Screening of phytochemicals as potent inhibitor
  of 3-chymotrypsin and papain-like proteases of SARS-CoV2: an in silico approach to
  combat COVID-19. *Journal of Biomolecular Structure and Dynamics*. 2020:1-15.
- 44. Yan H, Yu C. Repair of full-thickness cartilage defects with cells of different origin in
  a rabbit model. *Arthroscopy: The Journal of Arthroscopic & Related Surgery*.
  2007;23(2):178-187.
- 45. Zuker M. Mfold web server for nucleic acid folding and hybridization prediction.
   *Nucleic acids research*. 2003;31(13):3406-3415.
- 46. Huston NC, Wan H, Tavares RdCA, Wilen C, Pyle AM. Comprehensive in-vivo
  secondary structure of the SARS-CoV-2 genome reveals novel regulatory motifs and
  mechanisms. *BioRxiv*. 2020.
- 637 47. Rane JS, Chatterjee A, Kumar A, Ray S. Targeting SARS-CoV-2 Spike Protein of
  638 COVID-19 with Naturally Occurring Phytochemicals: An in Silco Study for Drug
  639 Development. In: ChemRxiv; 2020.
- 640 48. Souza PF, Lopes FE, Amaral JL, Freitas CD, Oliveira JT. A molecular docking study
  641 revealed that synthetic peptides induced conformational changes in the structure of

642		SARS-CoV-2 spike glycoprotein, disrupting the interaction with human ACE2
643		receptor. International journal of biological macromolecules. 2020;164:66-76.
644	49.	Elfiky AA. Ribavirin, Remdesivir, Sofosbuvir, Galidesivir, and Tenofovir against
645		SARS-CoV-2 RNA dependent RNA polymerase (RdRp): A molecular docking study.
646		Life sciences. 2020:117592.
647	50.	Aftab SO, Ghouri MZ, Masood MU, et al. Analysis of SARS-CoV-2 RNA-dependent
648		RNA polymerase as a potential therapeutic drug target using a computational
649		approach. Journal of translational medicine. 2020;18(1):1-15.
650	51.	Phan T. Genetic diversity and evolution of SARS-CoV-2. Infection, genetics and
651		evolution. 2020;81:104260.
652	52.	Belouzard S, Chu VC, Whittaker GR. Activation of the SARS coronavirus spike
653		protein via sequential proteolytic cleavage at two distinct sites. Proceedings of the
654		National Academy of Sciences. 2009;106(14):5871-5876.
655	53.	Korber B, Fischer W, Gnanakaran S, et al. Tracking changes in SARS-CoV-2 Spike:
656		evidence that D614G increases infectivity of the COVID-19 virus. Cell. 2020.
657	54.	Bhattacharyya C, Das C, Ghosh A, et al. SARS-CoV-2 mutation 614G creates an
658		elastase cleavage site enhancing its spread in high AAT-deficient regions. Infection,
659		Genetics and Evolution. 2021:104760.
660	55.	Perona JJ, Craik CS. Structural basis of substrate specificity in the serine proteases.
661		Protein Science. 1995;4(3):337-360.
662	56.	Fu Z, Thorpe M, Akula S, Chahal G, Hellman LT. Extended cleavage specificity of
663		human neutrophil elastase, human proteinase 3, and their distant ortholog clawed frog
664		PR3-three elastases with similar primary but different extended specificities and
665		stability. Frontiers in Immunology. 2018;9:2387.
666	57.	Li F. Structure, function, and evolution of coronavirus spike proteins. Annual review
667		of virology. 2016;3:237-261.
668	58.	Walls AC, Tortorici MA, Snijder J, et al. Tectonic conformational changes of a
669		coronavirus spike glycoprotein promote membrane fusion. Proceedings of the
670		National Academy of Sciences. 2017;114(42):11157-11162.
671	59.	Zhang L, Jackson CB, Mou H, et al. SARS-CoV-2 spike-protein D614G mutation
672		increases virion spike density and infectivity. Nature communications. 2020;11(1):1-
673		9.
674	60.	Weissman D, Alameh M-G, de Silva T, et al. D614G spike mutation increases SARS
675		CoV-2 susceptibility to neutralization. Cell host & microbe. 2021;29(1):23-31. e24.
676	61.	Wrapp D, Wang N, Corbett KS, et al. Cryo-EM structure of the 2019-nCoV spike in
677		the prefusion conformation. Science. 2020;367(6483):1260-1263.
678	62.	Hillen HS, Kokic G, Farnung L, Dienemann C, Tegunov D, Cramer P. Structure of
679		replicating SARS-CoV-2 polymerase. Nature. 2020:1-6.
680	63.	Yin W, Mao C, Luan X, et al. Structural basis for inhibition of the RNA-dependent
681		RNA polymerase from SARS-CoV-2 by remdesivir. Science. 2020.
682	64.	Kirchdoerfer RN, Ward AB. Structure of the SARS-CoV nsp12 polymerase bound to
683		nsp7 and nsp8 co-factors. <i>Nature communications</i> . 2019;10(1):1-9.
684	65.	Gao Y, Yan L, Huang Y, et al. Structure of the RNA-dependent RNA polymerase
685		from COVID-19 virus. Science. 2020;368(6492):779-782.
686	66.	Chand GB, Banerjee A, Azad GK. Identification of novel mutations in RNA-
687		dependent RNA polymerases of SARS-CoV-2 and their implications on its protein
688		structure. <i>bioRxiv</i> . 2020.
689	67.	Eskier D, Karakülah G, Suner A, Oktay Y. RdRp mutations are associated with
		- A

690 SARS-CoV-2 genome evolution. *bioRxiv*. 2020.

68. 691 Kern DM, Sorum B, Hoel CM, et al. Cryo-EM structure of the SARS-CoV-2 3a ion 692 channel in lipid nanodiscs. BioRxiv. 2020. 693 69. Malasics A, Gillespie D, Nonner W, Henderson D, Eisenberg B, Boda D. Protein 694 structure and ionic selectivity in calcium channels: Selectivity filter size, not shape, 695 matters. Biochimica et Biophysica Acta (BBA)-Biomembranes. 2009;1788(12):2471-696 2480. 697 70. Naranjo D, Moldenhauer H, Pincuntureo M, Díaz-Franulic I. Pore size matters for 698 potassium channel conductance. Journal of General Physiology. 2016;148(4):277-699 291. 700 71. Stephens RF, Guan W, Zhorov BS, Spafford JD. Selectivity filters and cysteine-rich 701 extracellular loops in voltage-gated sodium, calcium, and NALCN channels. 702 Frontiers in Physiology. 2015;6:153. 703 72. Suárez-Delgado E, Islas LD. Ion Channels: A novel origin for calcium selectivity. 704 Elife. 2020;9:e55216. 705 73. Kondratskyi A, Kondratska K, Skryma R, Prevarskaya N. Ion channels in the 706 regulation of apoptosis. Biochimica et Biophysica Acta (BBA)-Biomembranes. 707 2015;1848(10):2532-2546. 708 74. Yue Y, Nabar NR, Shi C-S, et al. SARS-Coronavirus Open Reading Frame-3a drives 709 multimodal necrotic cell death. Cell death & disease. 2018;9(9):1-15. 710 75. Pinton P, Giorgi C, Siviero R, Zecchini E. Rizzuto R. Bcl-2 and Ca. 2006;2:1409-711 1418. 712 76. Nieva JL, Madan V, Carrasco L. Viroporins: structure and biological functions. 713 Nature Reviews Microbiology. 2012;10(8):563-574. 714 77. Ren Y, Shu T, Wu D, et al. The ORF3a protein of SARS-CoV-2 induces apoptosis in 715 cells. Cellular & molecular immunology. 2020:1-3. 716 78. Castaño-Rodriguez C, Honrubia JM, Gutiérrez-Álvarez J, et al. Role of severe acute 717 respiratory syndrome coronavirus viroporins E, 3a, and 8a in replication and 718 pathogenesis. MBio. 2018;9(3). 719 79. Boni MF, Lemey P. Evolutionary origins of the SARS-CoV-2 sarbecovirus lineage 720 responsible for the COVID-19 pandemic. Nature microbiology. 2020. 721 80. Halfmann PJ, Hatta M, Chiba S, et al. Transmission of SARS-CoV-2 in domestic cats. 722 New England Journal of Medicine. 2020. 723 81. Shi J, Wen Z, Zhong G, et al. Susceptibility of ferrets, cats, dogs, and other 724 domesticated animals to SARS-coronavirus 2. Science. 2020;368(6494):1016-1020. 725 82. Tylor S, Andonov A, Cutts T, et al. The SR-rich motif in SARS-CoV nucleocapsid 726 protein is important for virus replication. Canadian journal of microbiology. 727 2009;55(3):254-260. 728 83. Järvelin AI, Noerenberg M, Davis I, Castello A. The new (dis) order in RNA 729 regulation. Cell Communication and Signaling. 2016;14(1):9. 730 84. Kikkert M. Innate immune evasion by human respiratory RNA viruses. Journal of 731 innate immunity. 2020;12(1):4-20. 732 85. Kopecky-Bromberg SA, Martínez-Sobrido L, Frieman M, Baric RA, Palese P. Severe 733 acute respiratory syndrome coronavirus open reading frame (ORF) 3b, ORF 6, and 734 nucleocapsid proteins function as interferon antagonists. Journal of virology. 735 2007;81(2):548-557. 736 86. McBride R, Van Zyl M, Fielding BC. The coronavirus nucleocapsid is a 737 multifunctional protein. Viruses. 2014;6(8):2991-3018. 738 87. Sokalingam S, Raghunathan G, Soundrarajan N, Lee S-G. A study on the effect of 739 surface lysine to arginine mutagenesis on protein stability and structure using green 740 fluorescent protein. PloS one. 2012;7(7):e40410.

741	88.	Chang C-k, Hou M-H, Chang C-F, Hsiao C-D, Huang T-h. The SARS coronavirus
742		nucleocapsid protein-forms and functions. Antiviral research. 2014;103:39-50.
743	89.	Haynes C, Iakoucheva LM. Serine/arginine-rich splicing factors belong to a class of
744		intrinsically disordered proteins. Nucleic acids research. 2006;34(1):305-312.
745	90.	Carlson CR, Asfaha, J. B., Ghent, C. M., Howard, C. J, Hartooni, N., Safari, M, &
746		Morgan, D. O. Phosphoregulation of Phase Separation by the SARS-CoV-2 N Protein
747		Suggests a Biophysical Basis for its Dual Functions. <i>Molecular Cell.</i> 2020;11:025.
748	91.	Schuster NA. Using the nucleocapsid protein to investigate the relationship between
749		SARS-CoV-2 and closely related bat and pangolin coronaviruses. <i>BioRxiv</i> . 2020.
750	92.	de Haan CA, Rottier PJ. Molecular interactions in the assembly of coronaviruses.
751		Advances in virus research. 2005;64:165-230.
752	93.	Huston NC, Wan H, Strine MS, Tavares RdCA, Wilen CB, Pyle AM. Comprehensive
753		in vivo secondary structure of the SARS-CoV-2 genome reveals novel regulatory
754		motifs and mechanisms. Molecular cell. 2021;81(3):584-598. e585.
755	94.	Kristofich J, Morgenthaler AB, Kinney WR, et al. Synonymous mutations make
756		dramatic contributions to fitness when growth is limited by a weak-link enzyme.
757		<i>PLoS genetics</i> . 2018;14(8):e1007615.
758	95.	Mitra S, Ray SK, Banerjee R. Synonymous codons influencing gene expression in
759		organisms. Research and Reports in Biochemistry. 2016;6:57.
760	96.	Hurst KR, Ye R, Goebel SJ, Jayaraman P, Masters PS. An interaction between the
761		nucleocapsid protein and a component of the replicase-transcriptase complex is
762		crucial for the infectivity of coronavirus genomic RNA. Journal of virology.
763		2010;84(19):10276-10288.
764	97.	Hurst KR, Koetzner CA, Masters PS. Characterization of a critical interaction
765		between the coronavirus nucleocapsid protein and nonstructural protein 3 of the viral
766		replicase-transcriptase complex. Journal of virology. 2013;87(16):9159-9172.
767	98.	Serrano P, Johnson MA, Almeida MS, et al. Nuclear magnetic resonance structure of
768		the N-terminal domain of nonstructural protein 3 from the severe acute respiratory
769		syndrome coronavirus. Journal of virology. 2007;81(21):12049-12060.
770	99.	Du X, Wang Z, Wu A, et al. Networks of genomic co-occurrence capture
771		characteristics of human influenza A (H3N2) evolution. Genome research.
772		2008;18(1):178-187.
773	100.	Rimmelzwaan G, Berkhoff E, Nieuwkoop N, Smith DJ, Fouchier R, Osterhaus A.
774		Full restoration of viral fitness by multiple compensatory co-mutations in the
775		nucleoprotein of influenza A virus cytotoxic T-lymphocyte escape mutants. Journal
776		of general virology. 2005;86(6):1801-1805.
777	101.	Deng L, Liu M, Hua S, et al. Network of co-mutations in Ebola virus genome predicts
778		the disease lethality. Cell research. 2015;25(6):753-756.
779	102.	Chen H, Zhou X, Zheng J, Kwoh C-K. Rules of co-occurring mutations characterize
780		the antigenic evolution of human influenza A/H3N2, A/H1N1 and B viruses. BMC
781		medical genomics. 2016;9(3):69.
782	103.	Rimmelzwaan GF, Kreijtz JH, Bodewes R, Fouchier RA, Osterhaus AD. Influenza
783		virus CTL epitopes, remarkably conserved and remarkably variable. Vaccine.
784		2009;27(45):6363-6365.
785	104.	Lyons DM, Lauring AS. Mutation and epistasis in influenza virus evolution. Viruses.
786		2018;10(8):407.
787	105.	Mohamed MM, El-Shimy IA, Hadi MA. Neutrophil Elastase Inhibitors: A potential
788		prophylactic treatment option for SARS-CoV-2-induced respiratory complications?
789		In: BioMed Central; 2020.

- Smith EC, Sexton NR, Denison MR. Thinking outside the triangle: replication fidelity
  of the largest RNA viruses. *Annual Review of Virology*. 2014;1:111-132.
- Pfeiffer JK, Kirkegaard K. Increased fidelity reduces poliovirus fitness and virulence
  under selective pressure in mice. *PLoS Pathog.* 2005;1(2):e11.
- Vignuzzi M, Stone JK, Arnold JJ, Cameron CE, Andino R. Quasispecies diversity
  determines pathogenesis through cooperative interactions in a viral population. *Nature*. 2006;439(7074):344-348.
- 109. Lei J, Kusov Y, Hilgenfeld R. Nsp3 of coronaviruses: Structures and functions of a large multi-domain protein. *Antiviral research*. 2018;149:58-74.
- 110. Skjesol A, Skjæveland I, Elnæs M, et al. IPNV with high and low virulence: host immune responses and viral mutations during infection. *Virology journal*. 2011;8(1):1-14.
- 802 111. Schoeman D, Fielding BC. Coronavirus envelope protein: current knowledge.
  803 *Virology journal.* 2019;16(1):1-22.
- 804 112. Escors D, Ortego J, Laude H, Enjuanes L. The membrane M protein carboxy terminus
  805 binds to transmissible gastroenteritis coronavirus core and contributes to core
  806 stability. *Journal of virology*. 2001;75(3):1312-1324.
- 807 113. J Alsaadi EA, Jones IM. Membrane binding proteins of coronaviruses. *Future*808 *Virology*. 2019;14(4):275-286.
- 809 114. Bai Y, Yao L, Wei T, et al. Presumed asymptomatic carrier transmission of COVID810 19. *Jama*. 2020;323(14):1406-1407.
- 811 115. Quan-Xin L, Xiao-Jun T, Qiu-Lin S, et al. Clinical and immunological assessment of
   812 asymptomatic SARS-CoV-2 infections. *Nature medicine*. 2020.
- 813 116. McCallum M, De Marco A, Lempp F, et al. N-terminal domain antigenic mapping
  814 reveals a site of vulnerability for SARS-CoV-2. *bioRxiv*. 2021.
- 815 117. Zhang B-z, Hu Y-f, Chen L-l, et al. Mining of epitopes on spike protein of SARS816 CoV-2 from COVID-19 patients. *Cell research*. 2020;30(8):702-704.
- 817 118. Mateus J, Grifoni A, Tarke A, et al. Selective and cross-reactive SARS-CoV-2 T cell
  818 epitopes in unexposed humans. *Science*. 2020;370(6512):89-94.
- 819 119. Volz E, Mishra S, Chand M, et al. Transmission of SARS-CoV-2 Lineage B. 1.1. 7 in
  820 England: Insights from linking epidemiological and genetic data. *medRxiv*.
  821 2021:2020.2012. 2030.20249034.
- Muik A, Wallisch A-K, Sänger B, et al. Neutralization of SARS-CoV-2 lineage B.
  1.1. 7 pseudovirus by BNT162b2 vaccine–elicited human sera. *Science*. 2021.
- McCarthy KR, Rennick LJ, Nambulli S, et al. Recurrent deletions in the SARS-CoV2 spike glycoprotein drive antibody escape. *Science*. 2021.
- Kemp S, Collier D, Datir R, et al. Neutralising antibodies drive Spike mediated
  SARS-CoV-2 evasion (medRxiv). *bioRxiv*. 2020.

### 828 Table 1. The scores of HADDOCK, PRODIGY (ΔG and Kd (M) at 37.0 □) for RdRp/NSP8

829

### and Spike-Elastase docked complex.

Variables	types	RdRp/NSP8	Spike-Elastase
HADDOCK score	Wild	-82.2 +/- 7.8	-43.0 +/- 8.9
HADDOCK Score	Mutant	-118.3 +/- 2.5	-61.9 +/- 4.5
$\Delta G$ (kcal mol <sup>-1</sup> )	Wild	-10.6	-13.3
AG (Kcai moi )	Mutant	-10.5	-13.7
Kd (M) at 37.0 🗆	Wild	3.5E <sup>-08</sup>	$4.5E^{-10}$

	Mutant	3.9E <sup>-08</sup>	$2.3E^{-10}$
Number of interfacial contacts (ICs) per property	Wild Mutant	charged-charged (5); charged-polar (9); charged-apolar (15); polar-polar (2); polar-apolar (16); and apolar- apolar (21) charged-charged(5);charged-polar (16);charged-apolar (19); polar-polar (3);polar-apolar(15); apolar-apolar (23)	charged-charged (17);charged-polar (22);charged-apolar (32);polar- polar (5);polar-apolar (31); and apolar-apolar (23) charged-charged (13);charged-polar (18);charged-apolar (27);polar- polar (4); polar-apolar (28) and apolar-apolar (36)
Associated amino acids of Elastase-2 with possible	Wild	P323: Asp(112), Cys(114), Val(115) and Pro (116)	<ul> <li>605 (Ser) and 607 (Gln): 36 (Arg);</li> <li>618 (Thr): 199 (Phe); 619 (Glu):</li> <li>199 (Phe), Cys (227); 620 (Val):</li> <li>198 (Cys), 225:227(Gly, Gly, Cys)</li> </ul>
docking interactions (for spike) or NSP8 (for RdRp)	actions (for e) or NSP8 Mutant	P323: Asp(112), Cys(114), Val(115) and Pro (116)	614 (Gly): 101 (Val); 618 (Thr): 181 (Arg), 223-226(Val, Arg, Gly, Gly); 619 (Glu): 103 (Leu), 181(Arg), 222-225(Phe, Val, Arg, Gly), 236 (Ala); 620 (Val): 223-227 (Val, Arg, Gly, Gly, Cys)

830Table 2. Assess the effect of mutations on structural dynamics of NSP-12/ RDRP, Spike,831NS3 and N Protein of SARS CoV-2 using DynaMut. The value of  $\Delta\Delta G < 0$  indicates that

832 the mutation causes destabilization and  $\Delta\Delta G>0$  represents protein stabilization. For

833  $\Delta\Delta$ SVibENCoM, positive and negative value denotes the increase and decrease of molecular

834 flexibility, respectively.

Protein	Mutation	ΔΔG	ΔΔG	ΔΔG	ΔΔG	ΔΔG	ΔΔG	Results*	$\Delta\Delta S_{Vib}$
Name	with	DynaMut	ENCoM	mCSM	SDM	DUET	FoldX		ENCoM
	position	kcal/mol	kcal/mol	kcal/mol	kcal/mol	kcal/mol	(kcal/mol)		kcal.mol <sup>-</sup>
									<sup>1</sup> .K <sup>-1</sup>
RdRp	P323L	1.054	-0.441	-0.264	0.700	0.118	-0.733	Stabilizing	-0.551
Spike	D614G	-0.769	+0.408	-0.492	2.530	0.195	+0.289	Destabilizing	0.510
ORF3a	Q57H	0.275	-0.128	0.788	0.520	-0.464	-1.438	Stabilizing	-0.160
N	RG203-	-	-	-	-	-	-3.42262	Highly	-
Protein	04KR							Destabilizing	
N	A220V	0.109	0.458	-0.586	-1.460	-0.567	+1.6	Stabilizing	-0.572
protein									

835

\*The final result of the stability for each protein was determined based on the intra-molecular
interactome analysis

# Figure 1. Schematic diagram of SARS-CoV-2 replication in cell showcasing the related to S, N, ORF3a, RdRp, NSP3 and 5'-UTR based epistatic interactions.

840 The replication cycle starts with the ACE2 receptor binding of the spike glycoprotein (S) as 841 cornered at the top-left and finishes with the exocytosis at the top-right. The viruses which do 842 not carry G-, GH- and/or GR-featured mutations in the S, N, ORF3a, RdRp, NSP3 and 5'-843 UTR are denoted as the wild type where mutants contain those. Throughout the diagram, the 844 red and green color icons such as proteins, genome, and virion represent the wild and mutant 845 type, respectively. For a generalized virion, we used the blue color. Although this theme is 846 not show the co-infection of both types, which might occur in rare occasions, we showed the 847 comparative epistatic effects side-by-side fashion during the whole replication cycle that will 848 make it easy to grasp. Related figure(s) for each protein are shown in the enclosed box. To 849 mean the uncertainty or unknown effects of any mutant proteins/RNA structure, we used the 850 'question' mark in a pathway and on explanatory box. RdRp- RNA dependent RNA 851 polymerase; NSP14-proof-reading enzyme of SARS-CoV-2; ER- endoplasmic reticulum; 852 **ERGIC-** endoplasmic

853

854 Figure 2. Different structural and stability comparison of wild and mutant spike 855 protein. Structural superposition of wild and mutant spike proteins (a-b); conformation in the 856 S1-S2 (c) and S2'sites (d-e); representation of vibrational entropy energy change on the 857 mutant type structure (f); and interatomic interaction prediction of both wild (g) and mutant 858 (h) types. For Figure a-e, the gray and yellow color represent the wild and mutant protein, 859 respectively. (a) The downstream (617-636) of D614G in wild (green) and mutant (red) S 860 protein was focused. Overlapping of the wild  $(D_{614})$  and mutant  $(G_{614})$  S protein showed 861 conformational change in the 3D structures. (b) However, the conformational change are in 862 the loop region (618-632) of the proteins thus may potentially play role in interacting with 863 other proteins or enzymes, such as elastase-2 as we focused in this work. (c) No change was 864 found in the S1-S2 cleavage site (685-686), depicted in blue color, of the wild and mutant 865 protein. (d) Surface and (e) cartoon  $(2^{\circ})$  structure of the superimposed wild and mutant 866 proteins where the S2' (pink) is situated in surface region and do not show any change in

- accessibility in the residual loop region. (f) The mutant ( $G_{614}$ ) protein showed higher flexibility in the  $G^{614}$  (sticks) and its surroundings (red). The intra-molecular interaction determined the overall stability of the (g) wild and (h) mutant structure where  $C_{\beta}$  of  $D^{614}$
- 870 (aspartic acid at 614; green stick modelled) had two hydrophobic interaction with the benzene
- 871 rings. This intramolecular contacts stabilize the S protein of wild type and missing of this
- bond destabilize the mutant ( $G_{614}$ ) protein. The mutant protein has glycine at 614 which has
- 873 less chance of interacting with other neighboring amino acids due to its shorter and nonpolar
- 874 R-group. The color code representing the bond type is presented in each (g) and (h).
- 875 Figure 3. The molecular docking of wild and mutant with elastase-2. Both the (upper 876 figure) wild  $(D_{614})$  and (lower figure) mutant  $(G_{614})$  version of S protein was shown in golden 877 color whereas the elastase-2 docked to  $D_{614}$  and  $G_{614}$  in blue and green color, respectively. 878 The enlarged views of the docked site were shown in separate boxes. (a) The possible docked 879 residues (stick model) on the wild S protein (warm pink) and elastase-2 (green) are 618(Thr)-880 619(Glu)-620(Val) and 198(Cys)-199(Phe)-225:227 (Gly, Gly, Cys), respectively. The 881 aspartic acid at 614 is 17.3°A far away from the valine (101), apparently the nearest amino 882 acid of elastase-2 to the cleavage site (615-616). (b) The possible interacting residues (stick 883 model) on the mutant S protein (blue) and elastase-2 (warm pink) are 614(Gly)-618(Thr)-884 619(Glu)-620(Val) and 101(Val)-103(Leu)-181(Arg)-222:227(Phe, Val, Arg, Gly, Gly, Cys), 885 and 236 (Ala) respectively. In this case, the glycine at 614 is only 5.4°A far away from the 886 valine (101), the nearest amino acid of elastase-2 to the cleavage site (615-616).

887

888 Figure 4. (a) Both the wild and mutated spike protein had lower RMSD profile till 60ns, then 889 it rised and maintained steady state. Although the spike protein had higher degree of 890 deviation in RMSD profile than RdRp but they did not exceed 3.0Å. The RMSD from 891 demonstrated that mutant and wild RdRp protein complex has initial rise of RMSD profile 892 due to flexibility. Therefore, both RdRp complexes stabilized after 30ns and maintained 893 steady peak. The wild type RdRp complex had little bit higher RMSD peak than mutant 894 RdRp which indicates the more flexible nature of the wild type. (b) The spike protein 895 complex had similar SASA profile and did not change its surface volume and maintained 896 similar trend during the whole simulation time. The higher deviation of SASA indicates that 897 mutant and wild type RdRp had straight line but mutant structure had higher SASA profile 898 which indicates the protein complex had enlarged its surface area. Therefore, mutation in 899 RdRp protein leads to more expansion of the surface area than wild types as their average 900 SASA value had significant difference. (c) Mutated spike exhibits little more Rg profile than 901 the wild type which correlates with the comparative labile nature of the mutant. The higher 902 level of Rg value defines the loose packaging system and mobile nature of the protein 903 systems. The mutant RdRp had lower level of fluctuations and maintains its integrity in 904 whole simulation time. The wild type RdRp complexes had higher deviations and more 905 mobility than the mutant complex. (d) Any aberration in hydrogen bond number can lead to 906 a higher flexibility. Therefore, the mutant and wild spike protein exhibit same flexibility in 907 terms of H-bonding. The mutant RdRp protein had more hydrogen bonding than the wild 908 types, but they did not differentiate too much and relatively straight line was observed for the 909 protein.

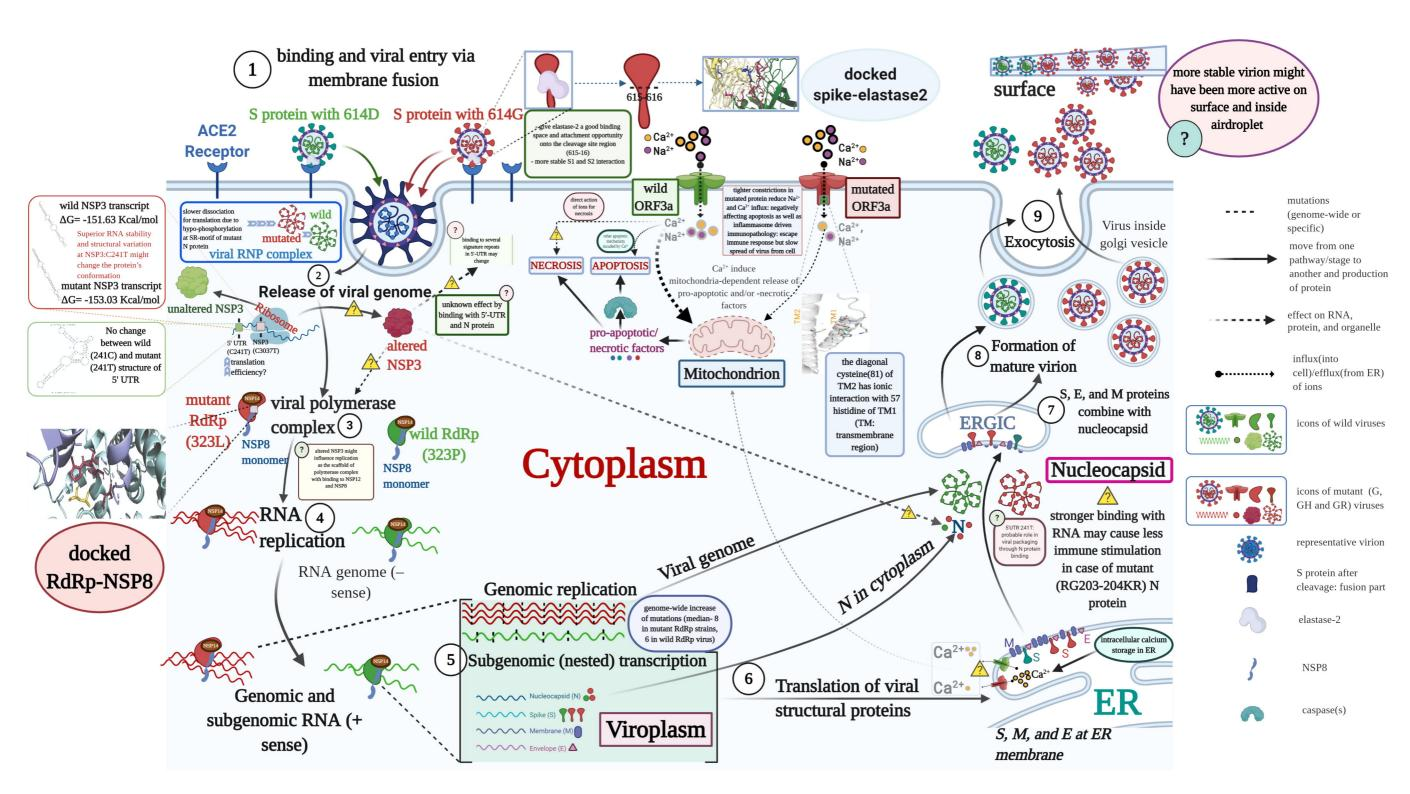
Figure 5. The molecular interaction of mutant RdRp with NSP8. The mutant ( $L_{323}$ ) RdRp (pale green) and NSP8 (light blue) are interacting as shown in center of the lower figure and an enlarged view of the docked site is presented above within a box. The leucine at 323 interacted with the Asp (112), Cys (114), Val (115), and Pro (116). The wild ( $P_{323}$ ) RdRp has identical docking interactions with NSP8 (table 4), thus is not presented as separate figure here.

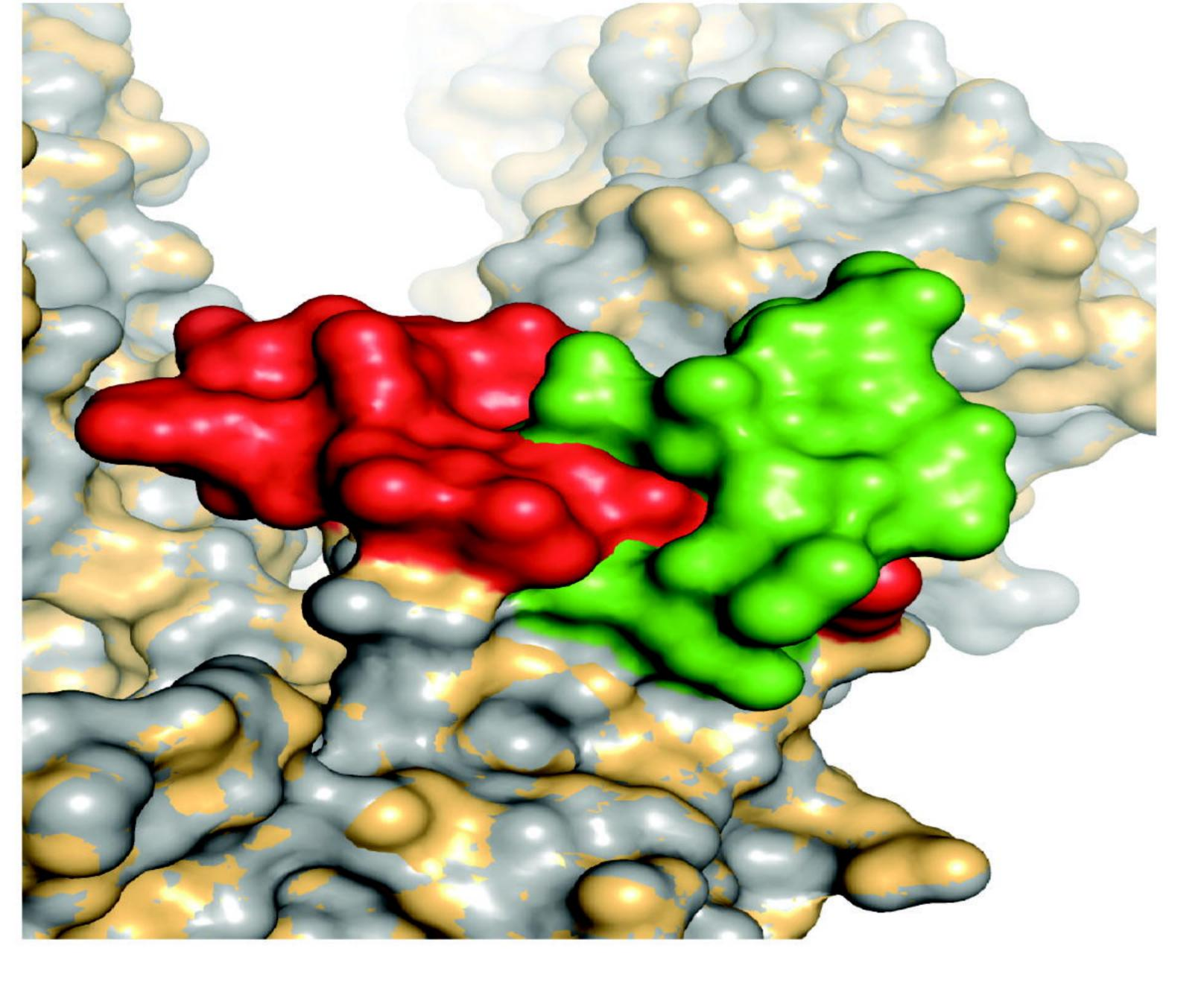
916 Figure 6. The effect on transmembrane channel pore of ORF3a viroporin due to 917 **p.Q57H mutation.** (a) The wild  $(Q_{57})$  and mutant  $(H_{57})$  ORF3a protein are presented in light 918 gray and green color, respectively. The structural superposition displays no overall 919 conformation change, however the histidine at 57 position of mutant ORF3a (deep blue) has 920 slightly rotated from glutamine at same position of the wild protein (bright red). This change 921 in rotamer state at 57 residue may influence (b) the overall stability of  $H_{57}$  (upper part) over 922  $Q_{57}$  (lower part) because of ionic interaction of histidine (green; stick model) of 923 transmembrane domain 1 (TM1) with cysteine at 81 (yellow stick) of TM2. The color code 924 defined different bond types is shown in inlet.

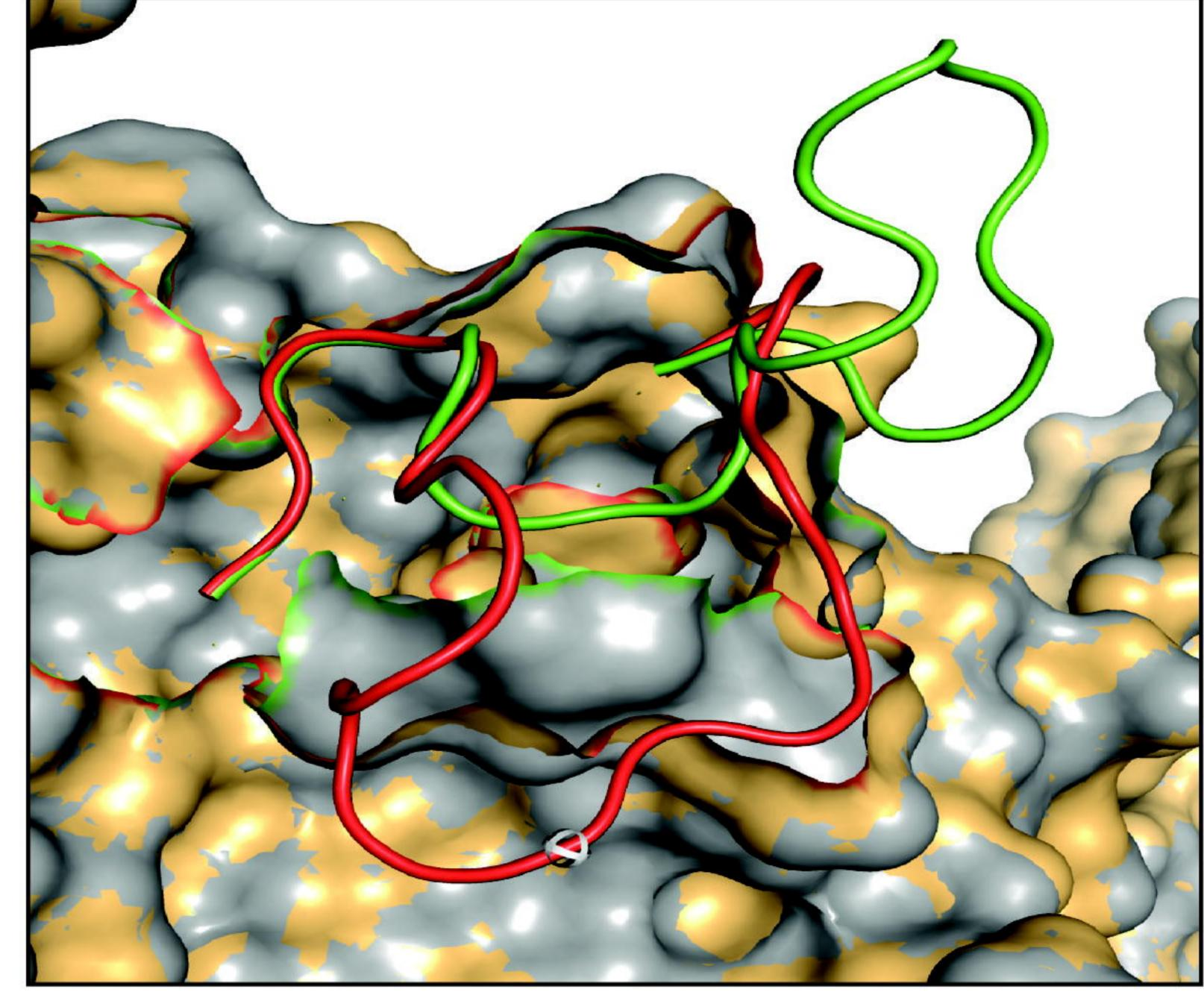
**Figure 7. Structural superposition of wild and mutant N protein.** The light grey color represents both wild ( $RG_{203-204}$ ) and mutant ( $KR_{203-204}$ ) N protein. The linker region (LKR: 183-247 amino acids) of wild ( $RG_{203-204}$ ) and mutant ( $KR_{203-204}$ ) are in pale yellow and warm pink color, respectively. (a) The aligned structures showed a highly destabilizing (Table 3) conformational change from 231 to 247 amino acids within LKR. Other regions of the N protein, especially the SR-rich region (184-204 amino acids) where the mutations occur, do

- 931 not change. (b) A more emphasized look into the SR-rich and mutated sites (RG203-204KR)
- 932 of wild and mutant N protein represent slight deviation in the Ser (197) and Thr (198) while
- 933 only glycine (green) to arginine (blue) substitution at 204 position shows changing at rotamer
- state. The enlarged view is shown in the bottom part.
- 935

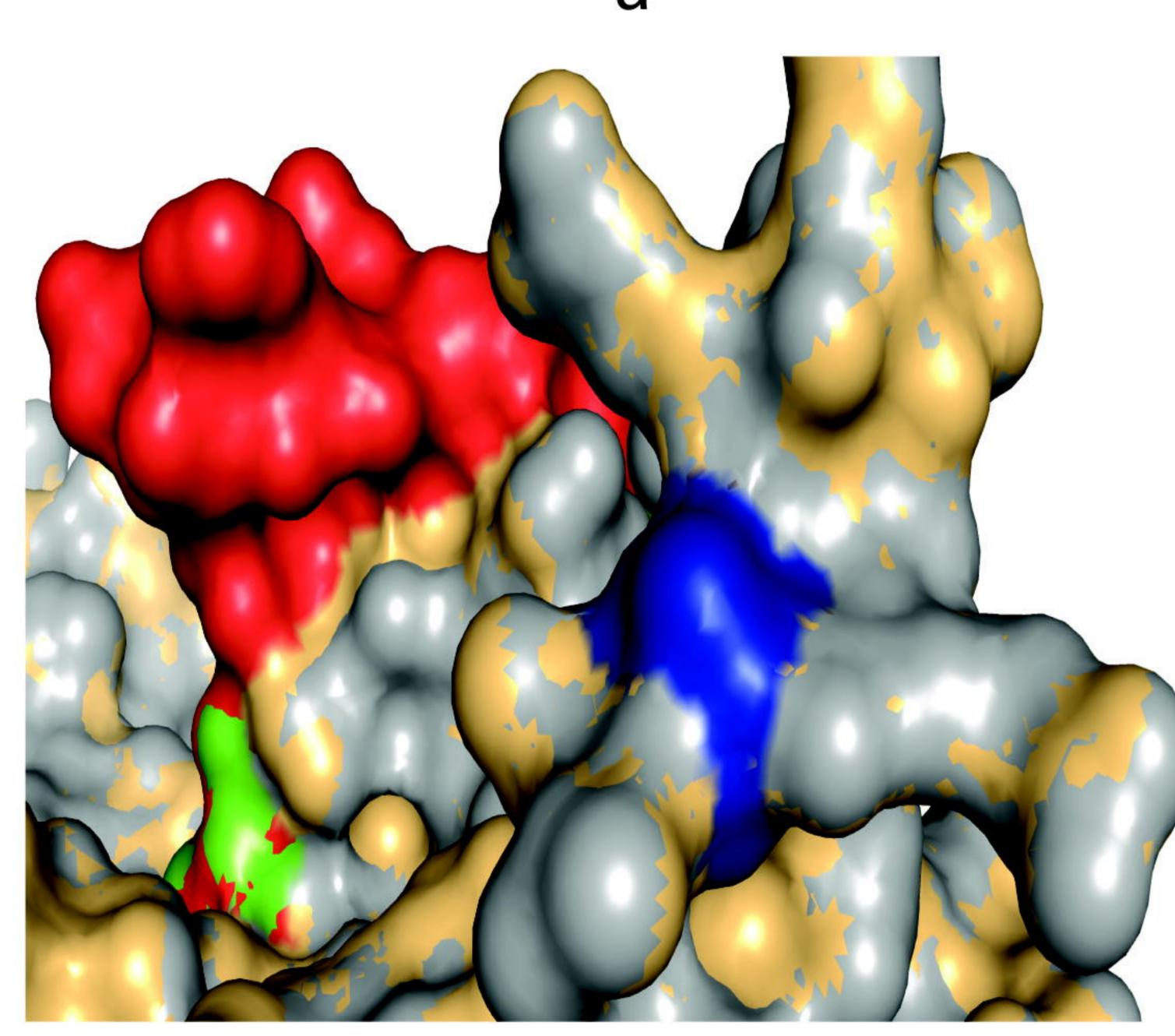
.

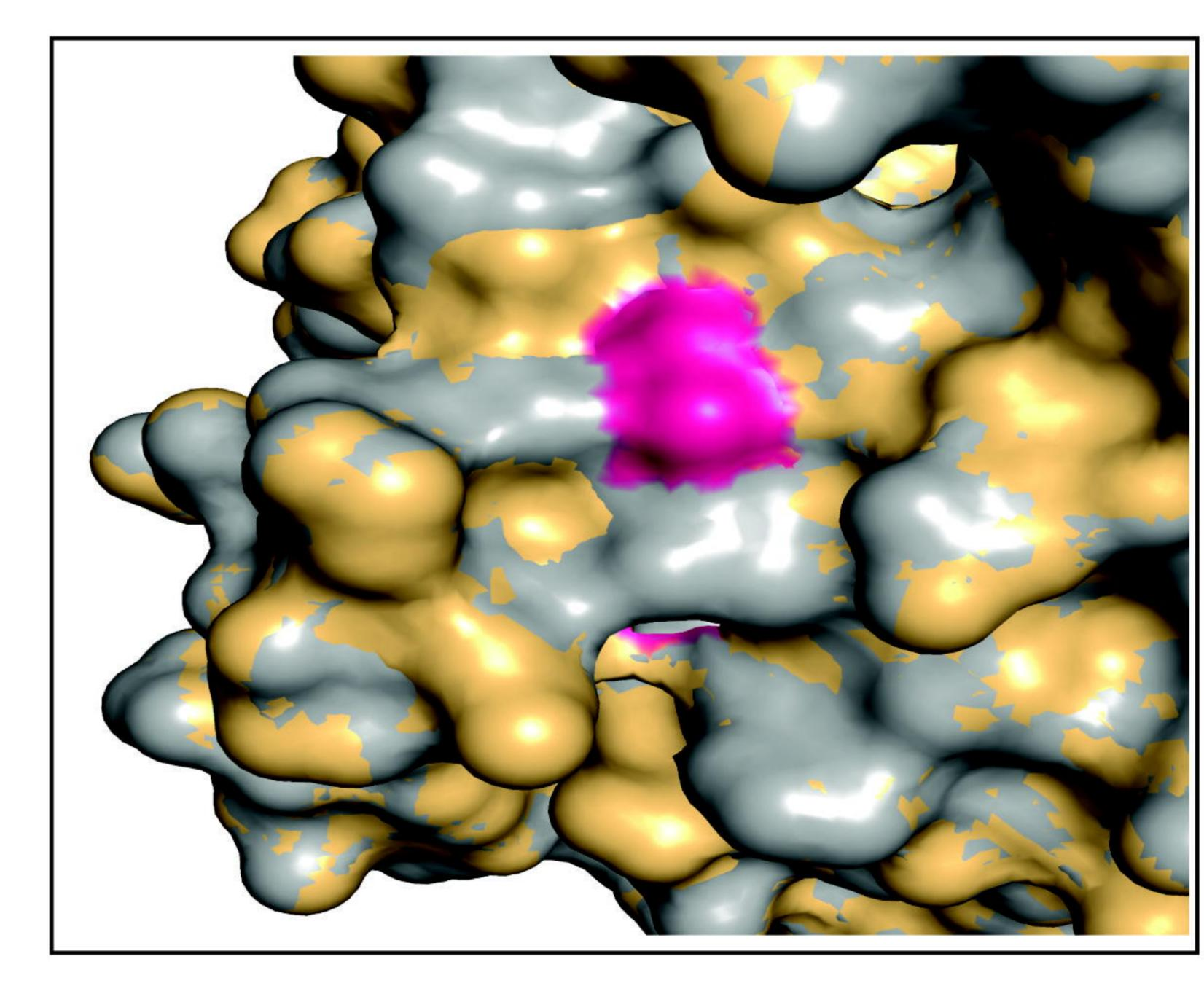


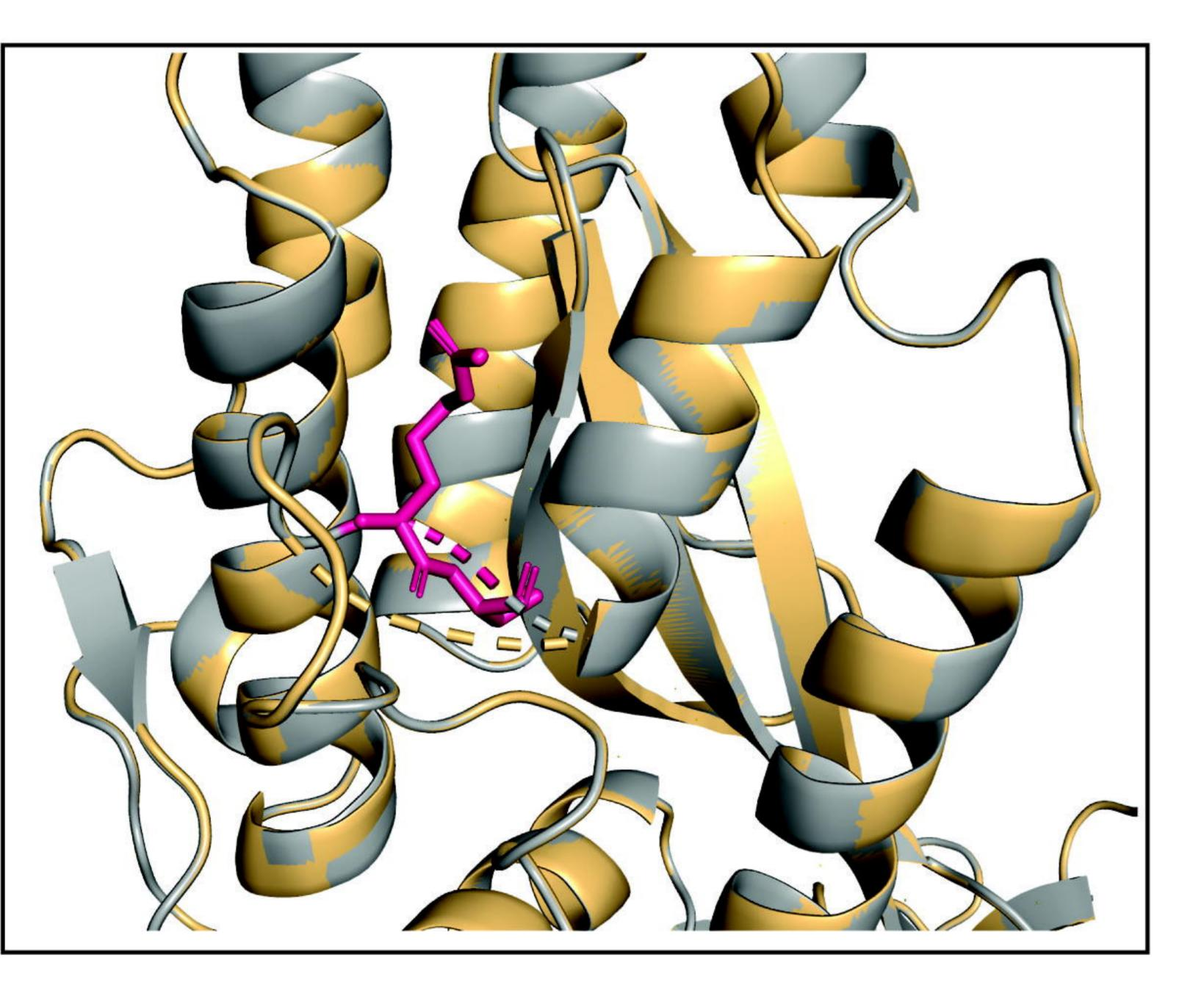


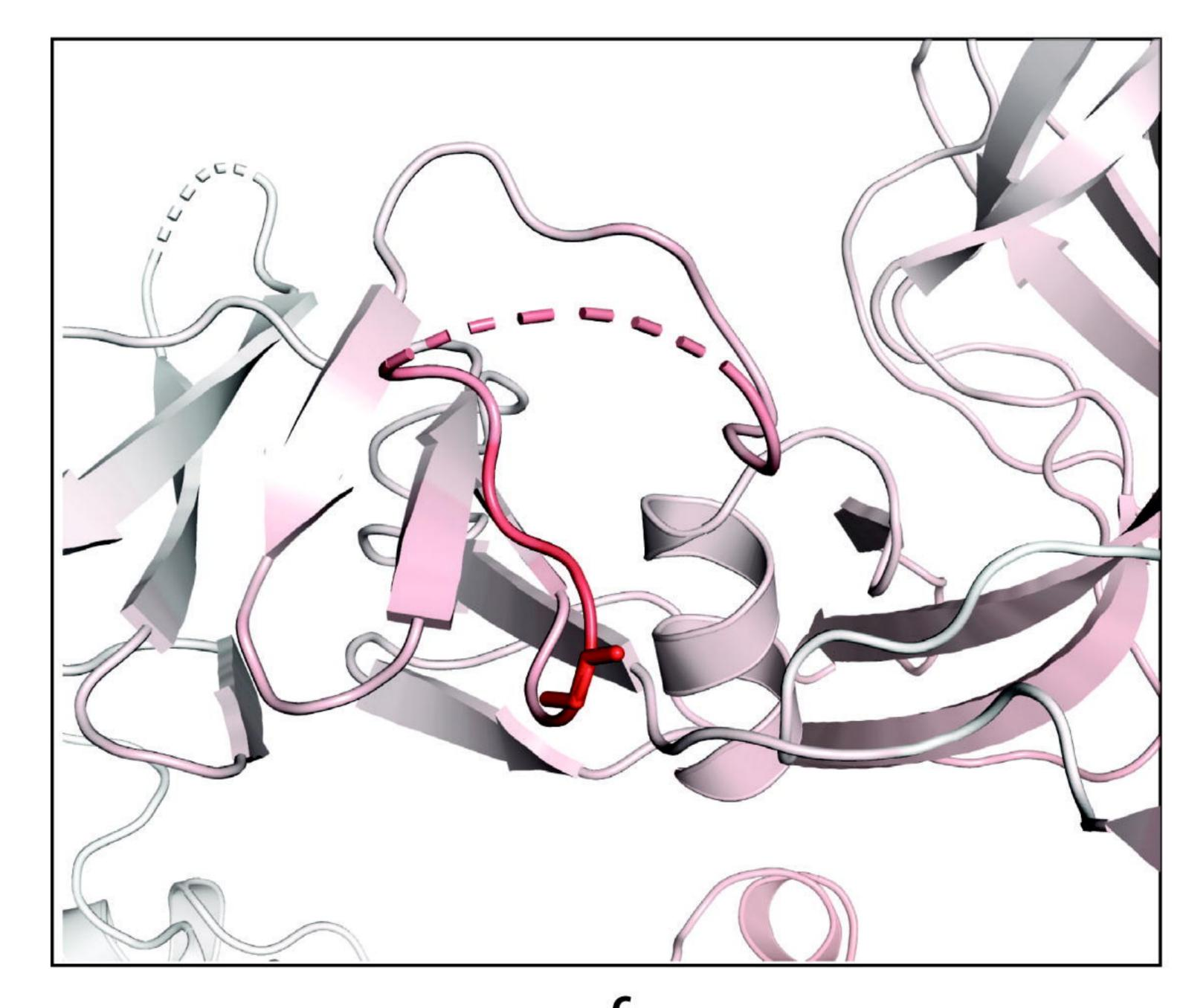


b

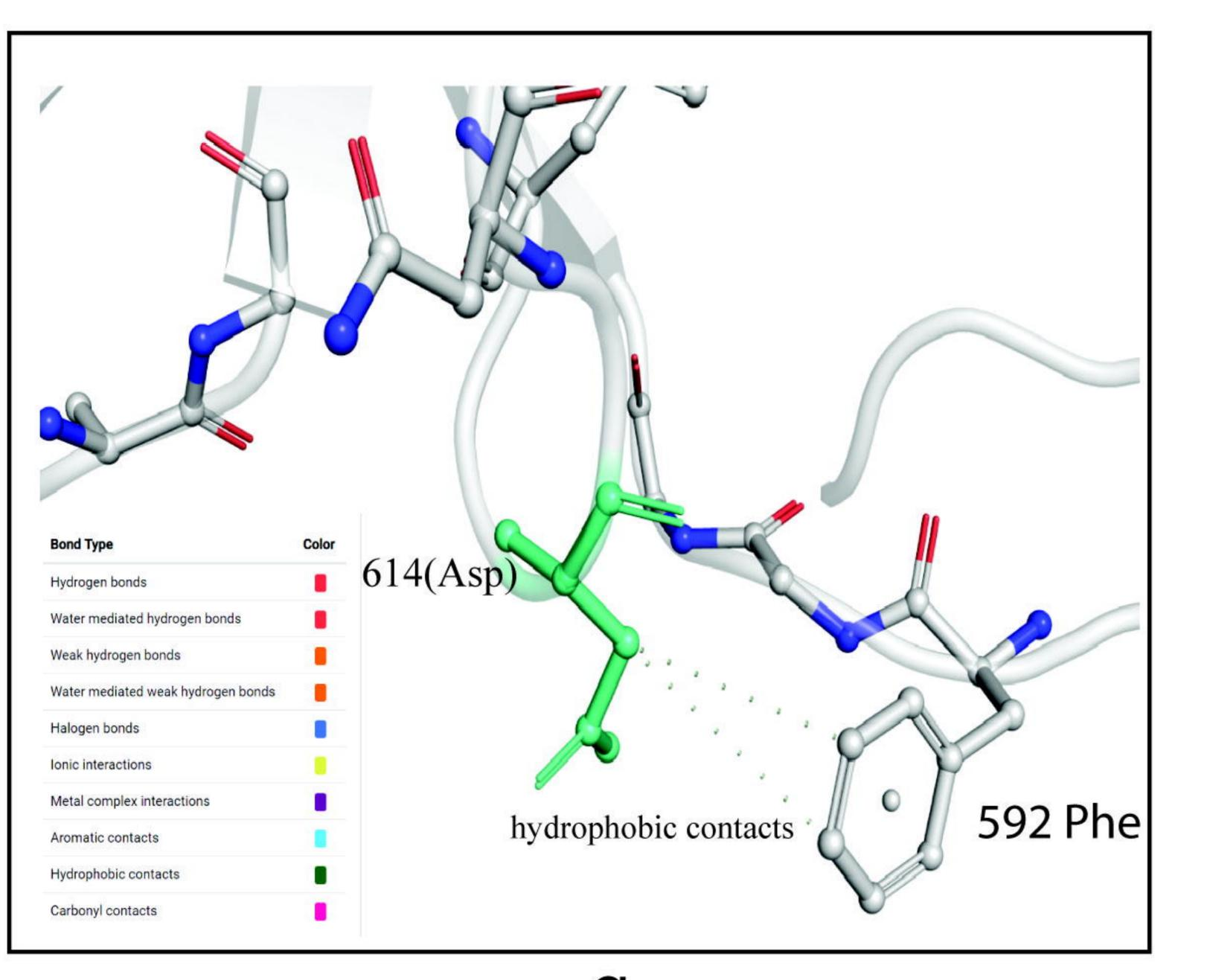


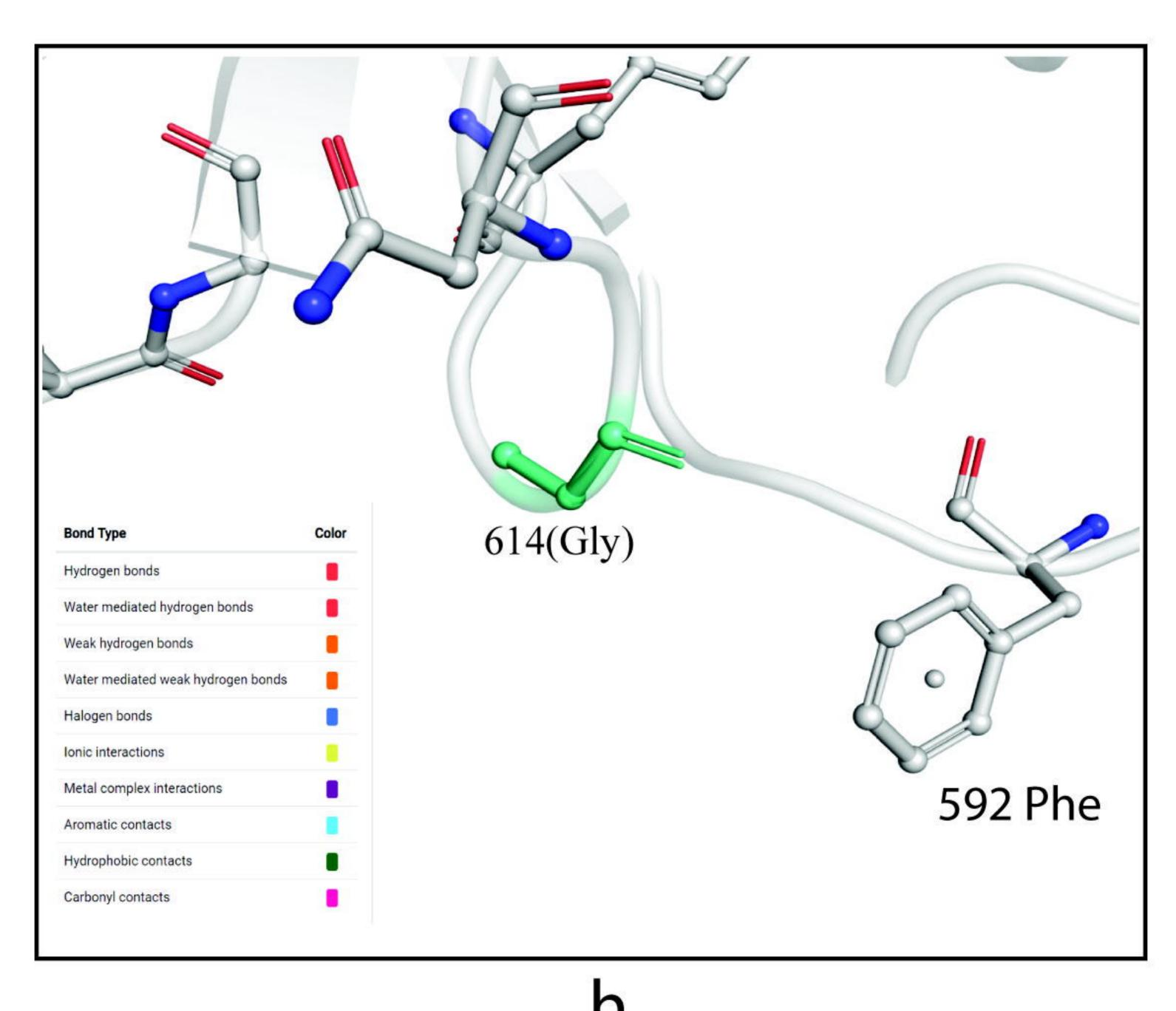


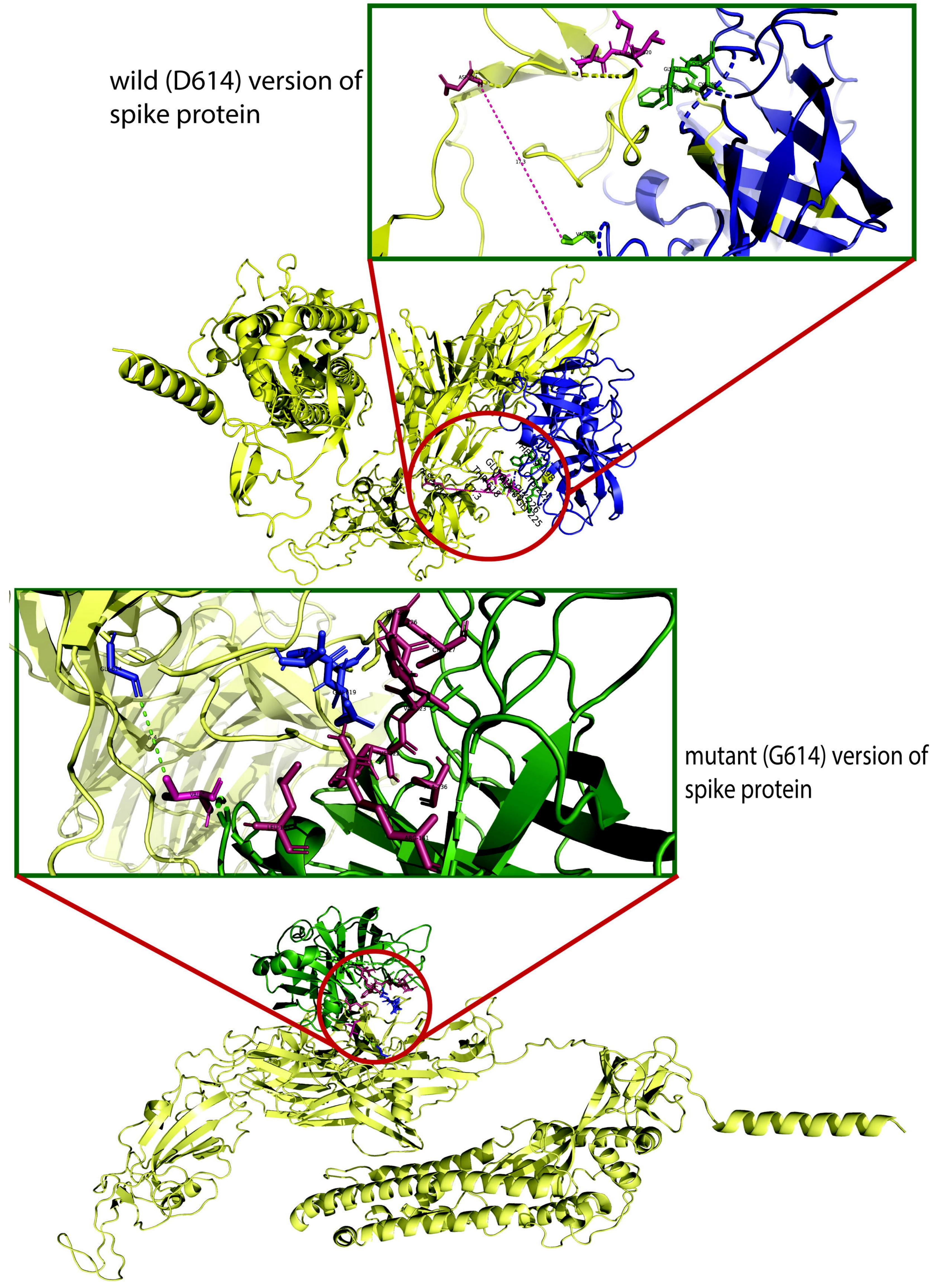


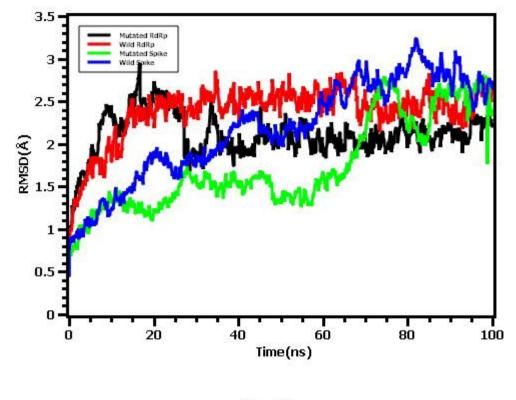


e

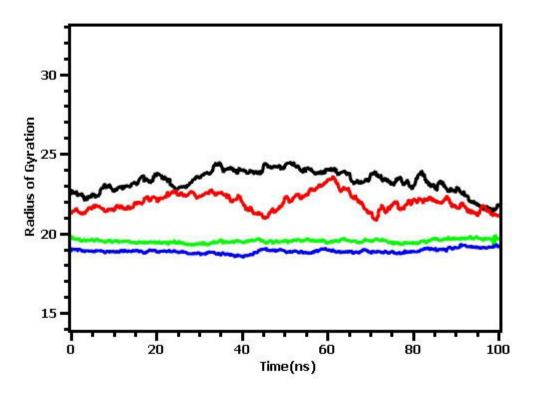


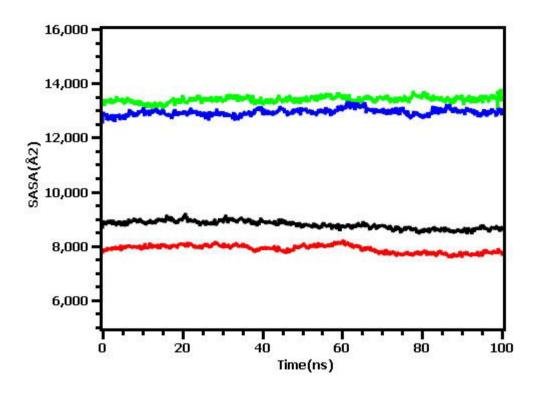




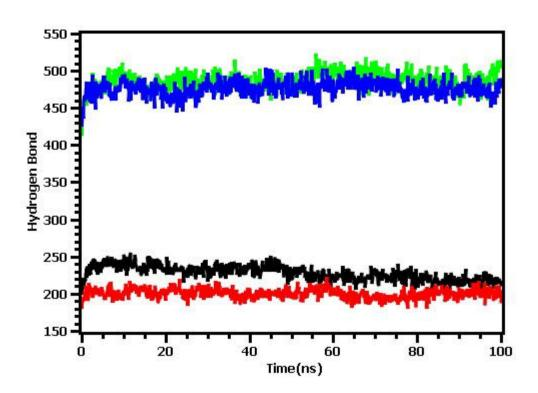


(a)



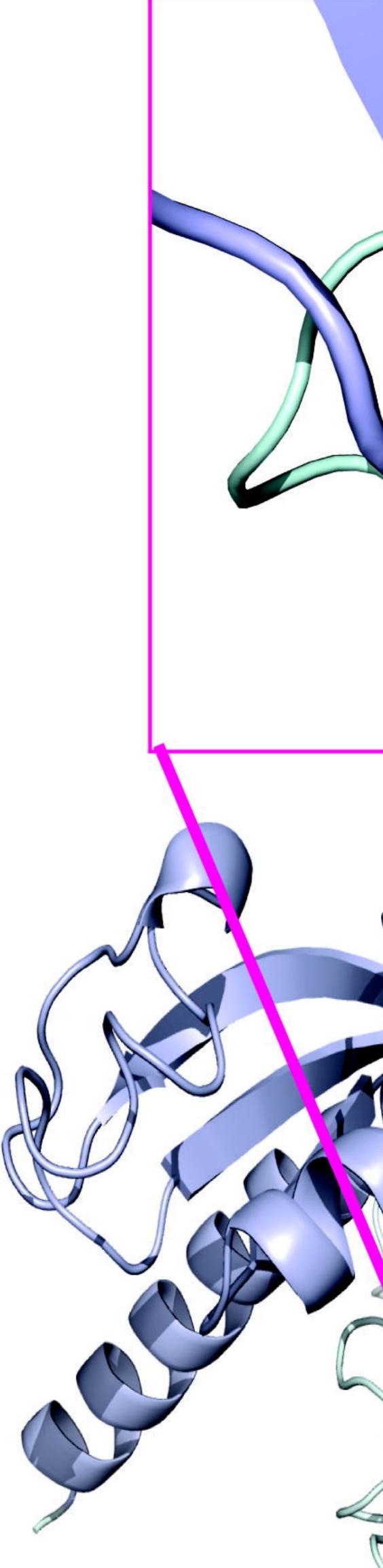


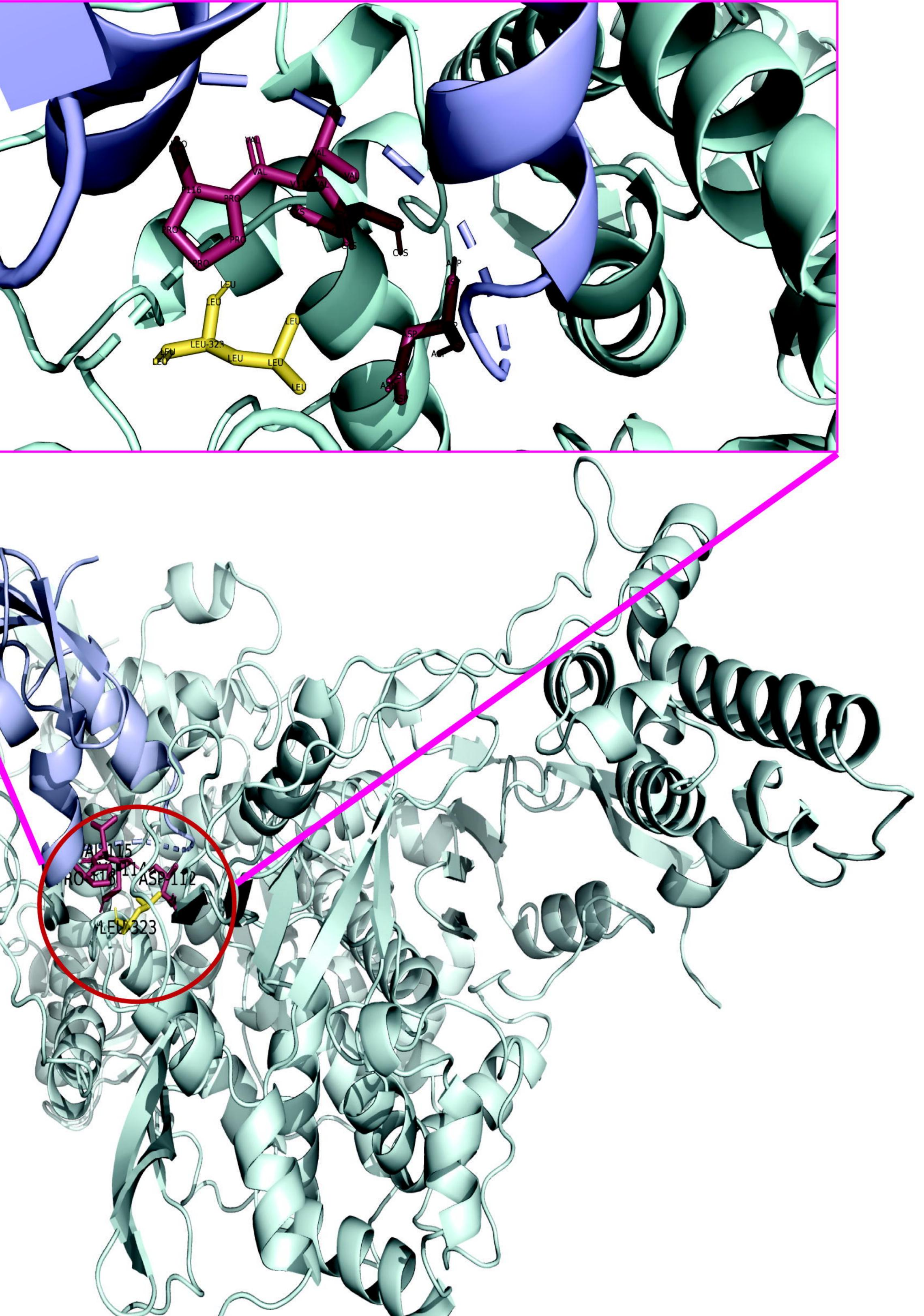
**(b)** 

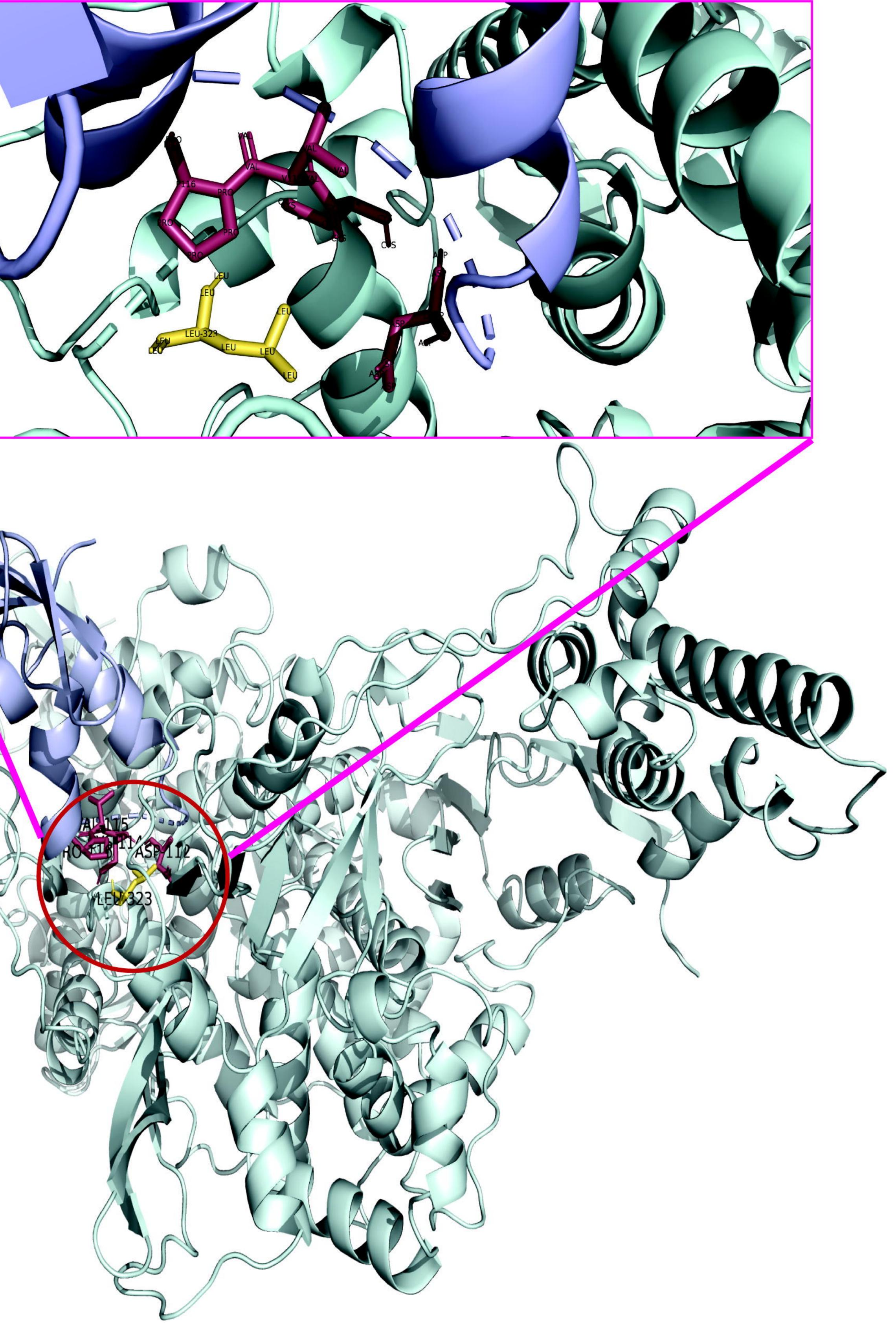


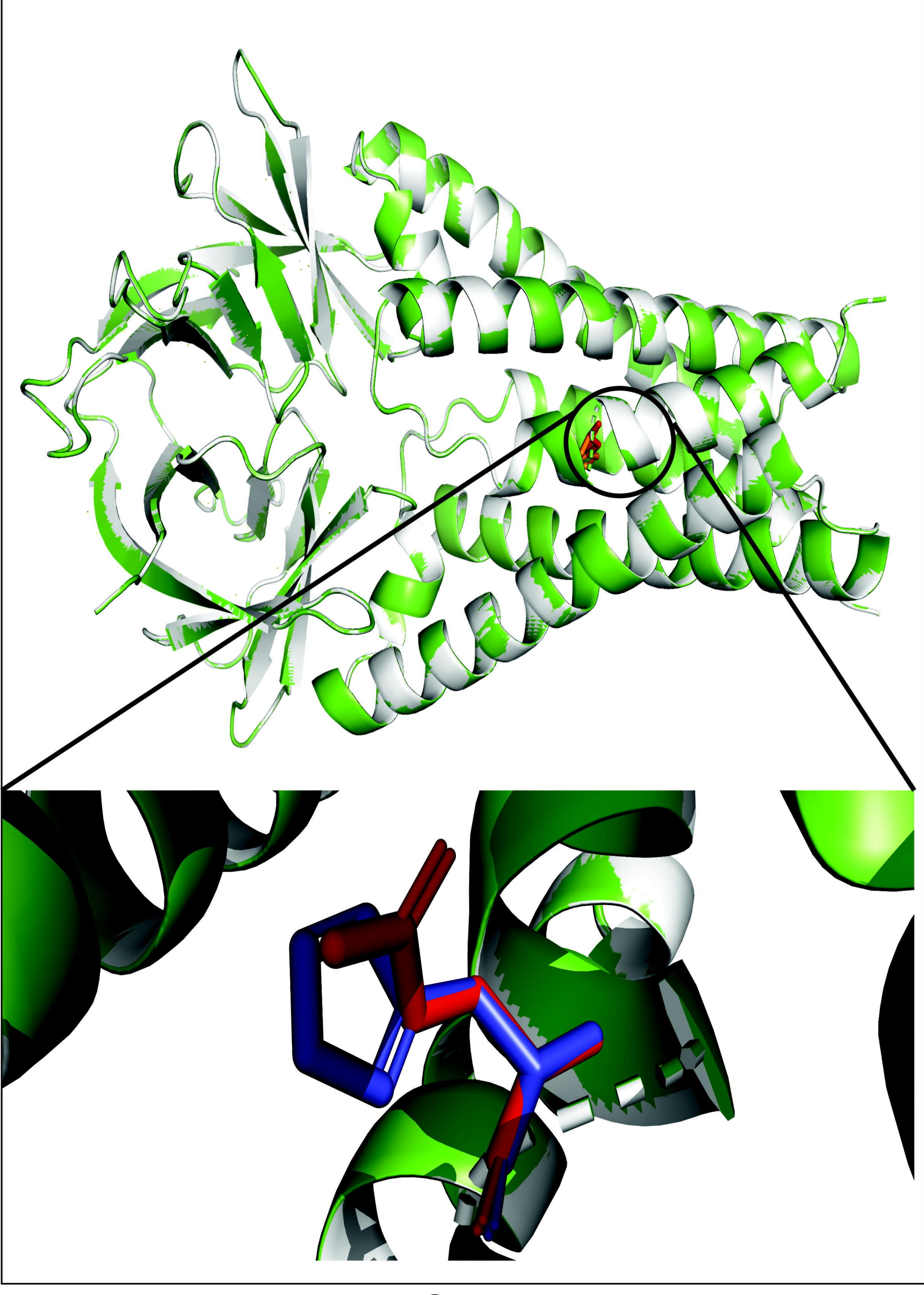
(d)

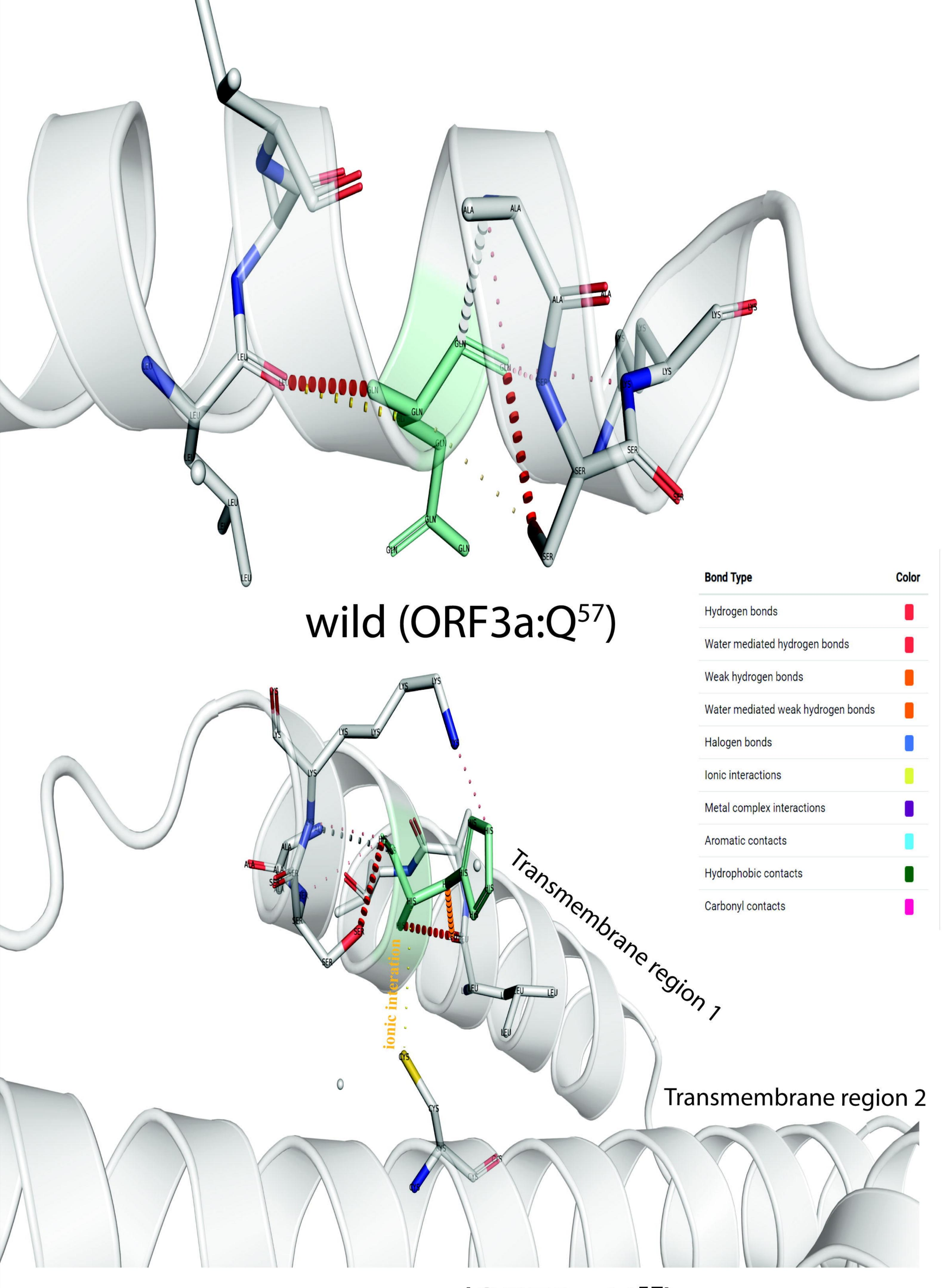
(C)











Bond Type	Color
Hydrogen bonds	
Water mediated hydrogen bonds	
Weak hydrogen bonds	
Water mediated weak hydrogen bonds	
Halogen bonds	
Ionic interactions	
Metal complex interactions	
Aromatic contacts	
Hydrophobic contacts	
Carbonyl contacts	



